Journal of Applied Fluid Mechanics, Vol. 17, No. 8, pp. 1657-1676, 2024.
Available online at www.jafmonline.net, ISSN 1735-3572, EISSN 1735-3645.
https://doi.org/10.47176/jafm.17.8.2451

Numerical Study of Solid–liquid Two-phase Flows and Erosion in a Y-type Slurry Valve with Different Seat Structures

G. Zhang[1, 2], H. Yi Zhang[1], J. L. Xin[1], D. S. Chen[1], and Z. Lin[1, 2†]

[1] *Key Laboratory of Fluid Transmission Technology of Zhejiang Province, Zhejiang Sci-Tech University, Hangzhou, 310018, China*
[2] *National-Provincial Joint Engineering Laboratory for Fluid Transmission System, Zhejiang Sci-Tech University, Hangzhou, 310018, China*

†Corresponding Author Email: linzhe0122@zstu.edu.cn

ABSTRACT

As a common industrial valve solution in slurry pipeline systems, Y-type slurry valves must be designed with properly shaped valve seat sealing rings to alleviate particle erosion and keep the valve operating in optimal condition. In this study, we investigate four different valve seat shapes with varying inner angles to understand the effect of the seat structure on particle erosion in Y-type slurry valves. We conducted computation fluid dynamics discrete element method simulations to analyze the impact of different valve seat shapes on the characteristics of particle–liquid two-phase flows and erosion. We also performed a detailed analysis of velocity and pressure distributions for liquid phase and particle velocity distributions as well as surface erosion on key valve components. We observed the primary erosion areas to be the back surface of the valve body, the inner surface of the valve seat, and the front surface of the valve disc, and as a result, we investigated the erosion distribution in these areas with different valve seat structures. Our simulation results indicate that the variation in particle diameter and the inner angle of the valve seat sealing ring have significant impacts on erosion in the studied areas.

Article History

Received November 27, 2023
Revised February 26, 2024
Accepted February 28, 2024
Available online May 29, 2024

Keywords:

Y-type slurry valve
Solid-liquid two-phase flows
Erosion
Seat structure
CFD-DEM

1. Introduction

Large-scale pipeline transportation is commonly used in modern industrial processes to transport slurry mixtures, and Y-type slurry valves are popular valve solutions used to control the flow state of the fluid medium in these processes. These valves find extensive applications across diverse sectors including petroleum and chemical processing, metallurgy, and water conservation. The longevity and operational efficacy of these valves have assumed heightened significance for ensuring the stability, safety, and economic viability of the overall production processes.

The Y-type slurry valve represents a prevalent industrial valve employed predominantly for the purpose of managing and governing fluid flow within pipelines. The critical components of the Y-type slurry valve are designed with a flow channel that diverges obliquely from the main pipeline. As a result, the resistance in the fluid is low, and this valve type is often used as a control valve for slurry transportation in industrial production. Many scholars have studied the two-phase flows, and in one example, Li et al. (2019) conducted an investigation into the flow characteristics of abrasive flow within a 90° stainless steel elbow, employing the large eddy simulation approach. The authors deliberated on the dual-phase flow distribution attributes of abrasive flow and elucidated the erosion characteristics exhibited by the primary wall. Tokura et al. (2019) examined the influence of particle deposition suspension modes on the solid–liquid mass transfer rate within a mechanically agitated vessel. They succinctly synthesized dimensionless equations characterizing the solid–liquid mass transfer rate under conditions of stagnation and complete suspension. Gu et al. (2019) employed computational fluid dynamics (CFD) to model the solid–liquid two-phase flow mixing dynamics across diverse impeller configurations. Their findings indicated a positive correlation between impeller speed and the homogeneity of fluid particle distribution, highlighting an enhanced uniformity with escalating impeller velocities. Singh et al. (2020) employed computational fluid dynamics (CFD) to simulate the intricate solid–liquid flow dynamics of coal–water slurry within the conical divergent section. Their simulations were subsequently experimentally validated, aiming to ascertain the optimal design parameters for the distributor. Chen et al. (2020) applied the Computational Fluid

Dynamics-Discrete Element Method (CFD-DEM) to model the particle collection process under varying initial motion conditions. Their investigation involved a detailed analysis of the intricate interplay between particles and fluid flow dynamics. Their results showed that the eddy current caused by the movement of the sphere was combined with that of the mainstream flow. Tang and Kim (2020) employed the CFD-DEM to model the distribution and motion attributes of solid particles within a single-channel pump. Their study systematically explored the impact of particle size and morphology on both particle velocity and spatial distribution. Lai et al. (2019) studied the influence of fluid velocity, different solid particle concentrations, and other factors on the flow and erosion of the pump and found that the impeller was the most seriously worn system component. Gopaliya and Kaushal (2022) proposed a correlation for predicting the local solid concentration of a horizontal pipe for the quasi-solid–liquid two-phase flow through Eulerian multiphase flow model simulation. Dumitrache and Hnatiuc (2018) designed a conical plug valve using a numerical simulation method to analyze the flow characteristics, such as velocity and pressure, of a circular port and a multi-circular port. They also used their simulation method to analyze the interaction between different fluid structures.

Erosion can be a serious issue in Y-type slurry valves because the liquid medium containing particles is likely to cause erosion, and in processes with solid–liquid two-phase flows, wall erosion can seriously degrade equipment safety. Ri et al. (2020) employed the discrete phase model (DPM) within CFD to scrutinize the fluid dynamics and erosion attributes in distinct valve configurations. Their investigation entailed the prediction of wall erosion rates induced by particles dispersed in solid–liquid two-phase flow. Zhang et al. (2019) numerically simulated an arrow check valve using CFD, predicted the distribution of erosion characteristics, and found the important factors affecting the flow field characteristics when the valve was open. Liu et al. (2021) numerically simulated a sewage valve based on CFD and analyzed the erosion conditions with different pressures, particle parameters, and particle concentrations, showing potentially serious erosion problems in sewage systems. Xu et al. (2022) orchestrated an erosion experiment for a ball valve, substantiating their findings by conducting a comparative analysis between numerical simulation data and experimental results. The results indicated that the orientation of the ball valve has a discernible impact on both the gravitational alignment and the distribution patterns of erosion along the inner wall of the valve. Lin et al. (2020) employed CFD-DEM to scrutinize the flow dynamics and erosion attributes within gate valves. The correlation with experimental data highlighted the existence of a high-velocity flow region beneath the gate, underscoring the pivotal role of particle concentration in shaping erosion rates. Ou et al. (2018) used CFD to numerically simulate a high-pressure coal water slurry valve and analyzed the failure mechanism of erosion, and their study pinpointed the apex of the spool head as the site of the highest erosion rate. Li et al. (2022a) applied the DPM to simulate the orifice of a valve, investigating the correlation between particle trajectories and erosion under diverse influencing factors. Their results showed that the factors affecting the erosion characteristics were related to the cone angle, pressure, flow rate, and particle parameters.

The valve seat of the Y-type slurry valve should also be designed to reduce fluid resistance and pressure loss, and to suppress erosion. The geometric configuration of the valve structure induces modifications in the adjacent flow field, exerting influence on the particle kinematics. This alteration in local structure further imparts adjustments to particle velocities and collision angles with the valve wall. Zhang et al. (2022) used the NSGA-II algorithm to optimize the structural parameters of the bionic valve. Their results showed that the cavitation area and length of these bionic structures were significantly reduced compared with traditional smooth structures. Their results also showed that the groove structure had the best cavitation resistance. Ou et al. (2022) applied CFD-DPM to conduct numerical simulations of erosion characteristics in solid–liquid two-phase flow within valves. They systematically altered the valve seat structure to influence fluid flow direction and regulate the resistance coefficient. The erosion rate was reduced by 79.7% after the flow channel interface was designed as a polygon. Liu et al. (2021) simulated an improved sewage valve structure by the CFD numerical simulation method and obtained the erosion distribution and rate, showing a reduced maximum erosion rate with the improved sewage valve. Yang et al. (2021) set up an anti-erosion device on the left wall of a throttle valve. They used CFD to design the anti-erosion device and analyzed the average velocity and erosion characteristics of the flow field. They achieved more stable flow velocity with the anti-erosion device, thereby reducing the erosion on the wall. Ou et al. (2018) proposed an improved valve core and downstream pipeline structure. They numerically simulated the valve interior through CFD and analyzed the erosion characteristics, showing reduced erosion for the valve core. Costa & Nara (2020) used CFD to simulate and calculate pipe elbows with various shapes and analyzed the erosion characteristics of the elbow part through numerical simulation. Their elbow shape design reduced the peak and range of erosion rates. Zheng et al. (2015) introduced a methodology for enhancing the structural design of ball valve seats through the utilization of CFD numerical simulations and calculated the velocity pressure, particle distribution, and erosion characteristic distribution. Their results showed that the range of wall erosion area became smaller after design improvements. Li et al. (2022b) employed CFD-DPM to investigate the erosion rates in elbows featuring hemispherical protrusions, and they found that a small protrusion angle and a large protrusion radius reduced the erosion rate of the elbow. Until now, the predominant focus of scholarly investigations has been on conventional valve types, notably ball valves and butterfly valves, and very few erosion studies have been performed for Y-type slurry valve seat structures. Consequently, a comprehensive exploration of the Y-type slurry valve seat structure becomes imperative to effectively mitigate erosion and uphold the optimal functionality of slurry pipeline systems.

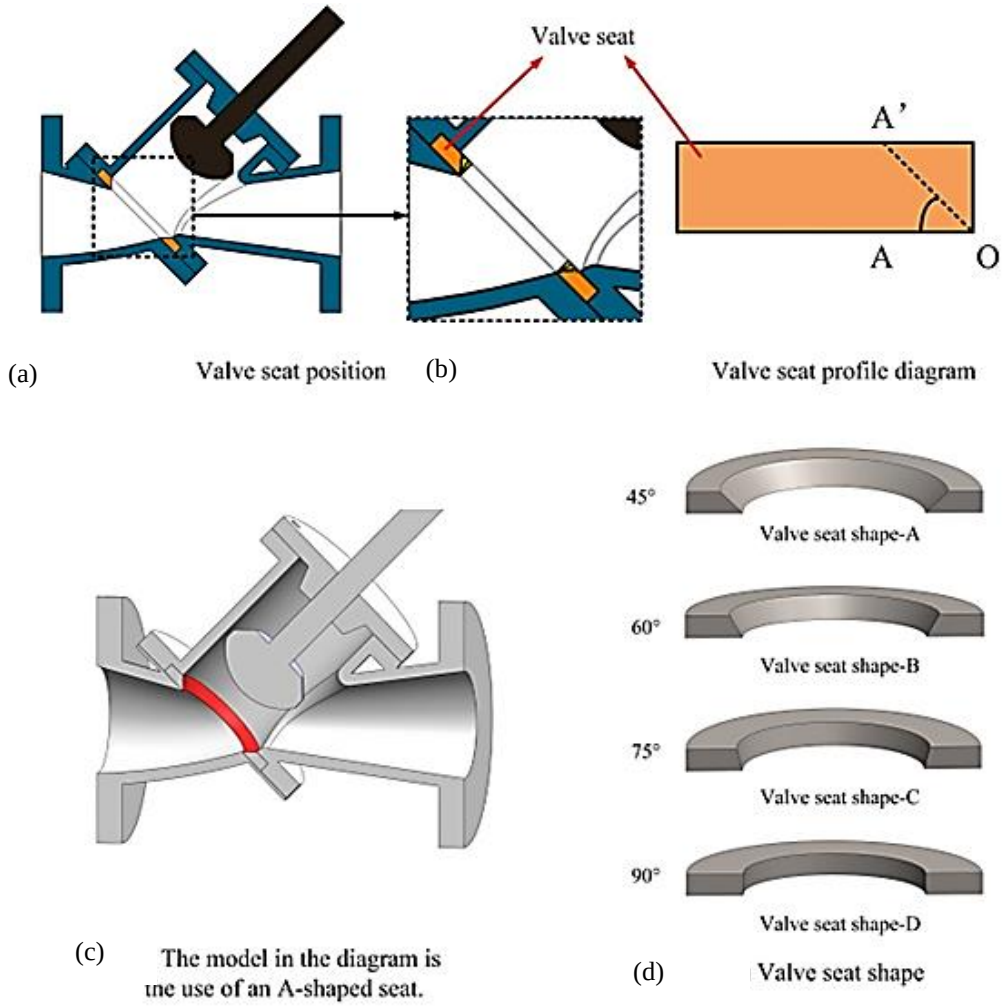

Fig. 1 Schematic of T-type slurry valve and design of valve seat shape

In a prior study (Zhang et al., 2023), we scrutinized the attributes of solid–liquid two-phase flow and the distribution of erosion within a Y-type slurry valve. This current investigation extends our previous work, focusing on the impact of different valve seat shapes on the efficacy of erosion suppression within the valve. We obtained liquid phase velocity and pressure distributions, and we discuss these distributions in detail as along with the particle velocity distribution. We analyze erosion distribution on the valve body's back surface, the valve seat's inner surface, and the valve disc's front surface with varying seat shapes, aiming to identify key erosion areas. Our study provides guidance for Y-type slurry valve designs to inhibit erosion, prolong valve service life, and ensure safe pipeline system operation.

2. COMPUTATIONAL MODEL AND NUMERICAL METHOD

2.1 Computational Model

We developed a three-dimensional computational Y-type slurry valve model with four valve seat sealing ring shapes, as depicted in Fig. 1. Figure 1(a) provides a schematic representation of the valve seat sealing ring positioning, accompanied by an enlarged view for detailed observation of the sealing ring configuration. Diverse configurations of the valve seat exert direct influence on the dimensions of the flow channel within the fluidic domain, the characteristics of solid–liquid two-phase flow, and the dynamic states of particles in motion. Figure 1(b) illustrates the longitudinal profile of the sealing ring. The right segment of the profile corresponds to the internal aspect of the valve seat sealing ring, and the O point sits toward the opening of the main pipe on the inner and upper sides of the sealing ring. The angle formed by the lower side and the inner side is defined as the angle AOA'. In Fig. 1(c), the red highlighted part of the model is the inner surface of the sealing ring, and we study four angles, 45° (shape A), 60° (shape B), 75° (shape C), and 90° (shape D), for AOA'. Three-dimensional illustrations of valve seats with these four angles are presented in Fig. 1(d).

We investigated the attributes of solid–liquid two-phase flows and particle erosion through numerical simulations, employing particle diameters of 50 μm and 250 μm, under a mass flow rate of 1.8 kg/s. We set the main pipe diameter, D, to 100 mm, and in simulation, we extended the pipe away from the valve by 15D in the upstream direction and 10D in the downstream direction to ensure a uniform distribution of particles in the liquid phase. The computational domain for the Y-type slurry valve is depicted in Fig 2.

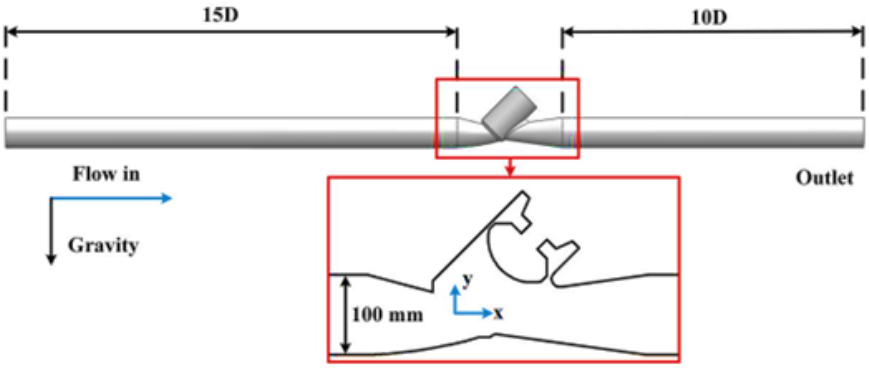

Fig. 2 Computational domain of numerical simulations

2.2 Numerical Method

We employed CFD-DEM within the ANSYS Fluent software to numerically compute the features of solid–liquid two-phase flows and erosion phenomena in Y-type slurry valves featuring distinct seat configurations. The realizable k-ε turbulence model was applied in conjunction with the E/CRC erosion model. Detailed descriptions of our specific numerical methodologies are provided in the subsequent subsections.

2.2.1 Turbulence Model

Turbulent flows contain many turbulent vortices, and the size and number of vortices will change with changes in the flow state and particle motion in the valve. Therefore, selecting an appropriate turbulence calculation model holds paramount significance in the numerical simulation process. Reynolds-averaged Navier–Stokes (RANS), based on statistical averaging of turbulence, is one of the most commonly used turbulence simulation methods and uses various turbulence models to describe the transport and dissipation of turbulence. The approach demonstrates rapid computational efficiency and comparatively high precision, rendering it applicable to a broad spectrum of engineering flow scenarios. Among the RANS solution methods, the realizable k-ε model has better physical realism and higher computational efficiency than other approaches, and this model can better describe complex flow phenomena, such as rotational effects and three-dimensional flow. Considering various factors, such as the three-dimensional structure of the Y-shaped slurry valve flow channel, actual calculation cost, and accuracy requirements, in ensuring the accuracy and reliability of our numerical outcomes, we opted for the realizable k-ε model, as advocated by Greitzer et al. (2004). This model may be represented as follows:

$$\frac{\partial(\rho k)}{\partial t}+\frac{\partial(\rho k u_i)}{\partial x_i}=\frac{\partial}{\partial x_j}\left[\left(\mu+\frac{\mu_t}{\sigma_k}\right)\frac{\partial k}{\partial x_j}\right]+G_k-\rho\varepsilon_k \quad (1)$$

$$\frac{\partial(\rho\varepsilon)}{\partial t}+\frac{\partial(\rho\varepsilon u_i)}{\partial x_i}=\frac{\partial}{\partial x_j}\left[\left(\mu+\frac{\mu_t}{\sigma_\varepsilon}\right)\frac{\partial k}{\partial x_j}\right]+C_1\rho S\varepsilon-C_2\rho\frac{\varepsilon^2}{k+\sqrt{\upsilon\varepsilon}} \quad (2)$$

In this formulation, G_k signifies the turbulent kinetic energy arising from the average velocity gradient, and $C_1=\max\left(0.43,\frac{\eta}{\eta+5}\right)$, υ is the kinematic viscosity, $C_2=1.9$

2.2.2 Calculation Model of Liquid Phase

The calculation model of liquid-phase flows is the basis for studying the behavior of fluid characteristics, and the incompressible RANS equations are utilized to model liquid-phase flows. The continuity equation and momentum conservation equation employed for solving the liquid-phase flows are outlined in the following paragraphs.

(1) Continuity Equation

The continuity equation expresses that the increase and decrease in working fluid mass must be equal in the inlet and outlet of the computational domain at any time. More specifically, the mass is conserved according to.

$$\nabla\cdot v=0 \quad (3)$$

Where v is the velocity of the fluid.

(2) Momentum Conservation Equation

Derived from Newton's second law, the momentum conservation equation portrays fluid motion influenced by various forces. The interaction between fluid and particles is included in the equation as

$$\frac{\partial V}{\partial t}+(V\cdot\nabla)V=-\frac{1}{\rho}\nabla P+\frac{\mu}{\rho}\nabla^2V-\nabla\cdot\tau_{ij}+\mathrm{g}-\sum F \quad (4)$$

In the aforementioned equation, P represents static pressure, V signifies liquid velocity, ρ denotes liquid density, τ_{ij} stands for the stress tensor, g represents gravitational acceleration, and F represents the resistance per unit mass (particle) between the fluid and the particle.

2.2.3 Calculation Model of Particle Phase

In solid–liquid two-phase flows, intricate interactions between solid particles and the liquid phase play a pivotal

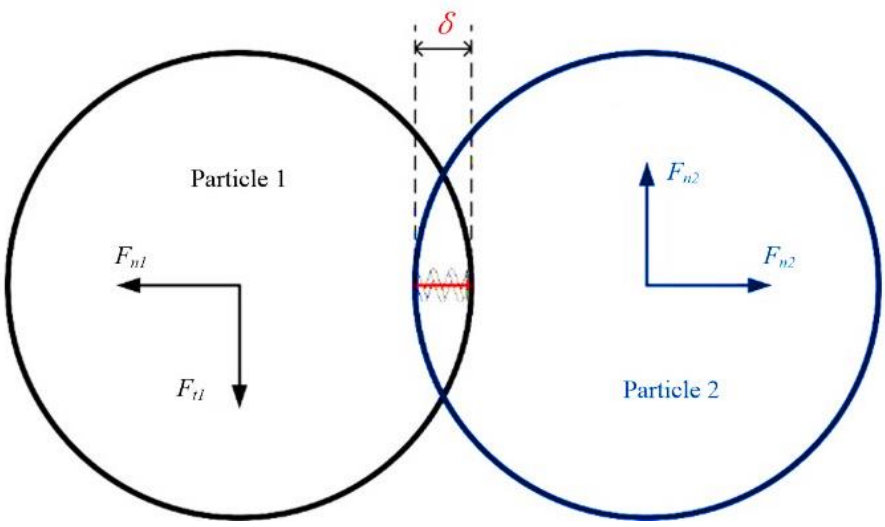

Fig. 3 Soft sphere model

role in shaping the flow field structure and governing particle dynamics. Concurrently, the occurrence of particle collisions and energy transfer adds complexity to the system dynamics. To describe these interactions, the particle momentum equation, particle collision contact force, and particle–wall collision and rebound model are outlined in the following paragraphs.

(1) Particle Momentum Equation

The particle momentum equation is a physical equation describing the momentum change in particles under the action of external force, representing the change rate of momentum. The equation governing particle momentum is articulated as follows:

$$\frac{\mathrm{d}V_p}{\mathrm{d}t} = \mathrm{g} + f_B + f_D + f_M + f_P + f_S + f_{VM} \tag{5}$$

Where V_p is the velocity vector of solid particles, g is the acceleration of gravity, and f_B, f_D, f_M, f_P, f_S and f_{VM} represent the Bassett force, drag force, Magnus force, pressure gradient force, Saffman force, and virtual mass force, respectively. All these forces are unit mass forces and are considered in the numerical model. The Basset force, drag force (Morsi & Alexander 1972), and Magnus force (Yamamoto et al., 2001) are the fundamental forces that describe the motion of particles in a fluid, with drag force being an important factor affecting particle velocity and distribution. The pressure gradient force mainly affects the motion of the fluid, but it also has an impact on the motion of particles. The Saffman force (Barati et al., 2014) is caused by the presence of a small amount of roughness on the surface of particles, which forms certain vortices during the liquid phase flow process and causes the particles to be subjected to a lateral force. The virtual mass force (Auton, et al., 1988) describes how particles are subjected to a certain virtual mass force due to their influence on the dynamic characteristics of the fluid.

(2) Particle Collision Contact Force

DEM serves as a numerical simulation methodology utilized for scrutinizing the mechanical responses of granular materials, encompassing particles and powders. In this study, we added the DEM soft sphere model to the calculation process, and the collision and motion between particles were simulated by establishing the interaction mechanical model between particles.

(3) Particle–Wall Collision and Rebound Model

In numerical simulations of Y-type slurry valves with solid–liquid phases, Considerations for particle-wall interactions, encompassing collision and rebound dynamics, are essential in the analysis. Particles colliding and rebounding with the flow channel wall incur momentum loss and modifications in rebound angle and velocity. The particle–wall rebound model, which plays a vital role in elucidating the rebound angle and velocity subsequent to particle impact, incorporates the elastic collision recovery coefficient introduced by Grant & Tabakoff (1975) in this investigation. The coefficient expressing elastic collision restitution is formulated as follows:

$$e_n = 0.993 - 1.76\theta + 1.56\theta^2 - 0.49\theta^3 \tag{6}$$

$$e_t = 0.988 - 1.66\theta + 2.11\theta^2 - 0.67\theta^3 \tag{7}$$

Where θ represents the incident angle, e_n represents the normal recovery coefficient, and e_t denotes the tangential recovery coefficient, both reflecting post-collision alterations in the particle's normal and tangential components.

2.2.4 Erosion Model

Considering the contact and friction between solid particles, pipeline walls, valves, and other equipment, the application of erosion models becomes particularly important. Considering factors such as friction and impact between particles and the valve surface, the erosion rate of the valve wall and the erosion degree of particles can be

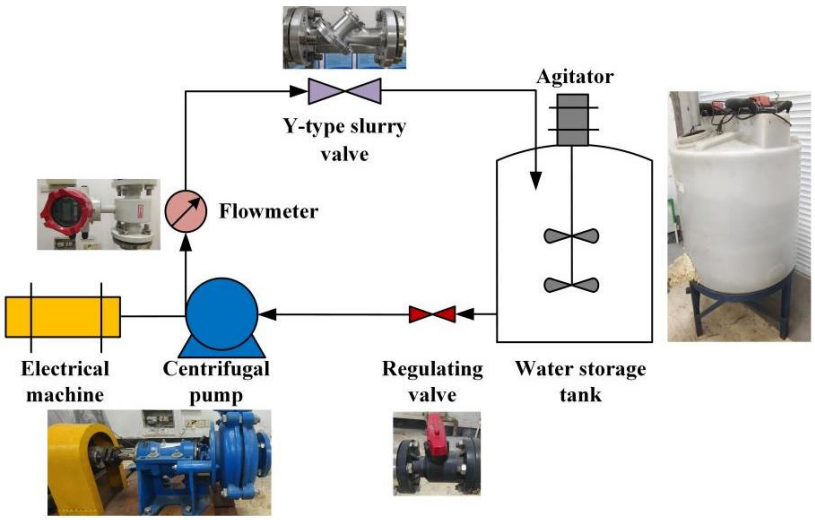

(a)

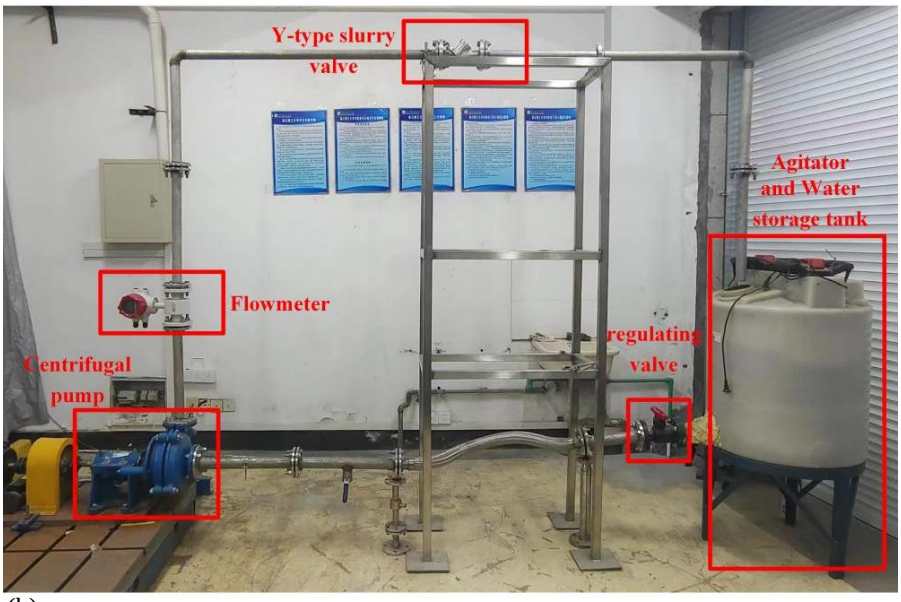

(b)

Fig. 4 Experimental system

calculated. Choosing an appropriate erosion model can provide a scientific basis for predicting valve service life, optimizing process parameters and improving the valve structure. In this investigation, we utilized the E/CRC erosion model, introduced by Zhang et al. (2007), to calculate the erosion rate, formulated as follows:

$$ER = C(BH)^{-0.59} F_s u_p^{n_c} f(\theta) \tag{8}$$

$$f(\theta) = \sum_{i=1}^{5} R_i \theta^i \tag{9}$$

where ER denotes the erosion rate, characterized as the quotient of wall mass loss to the mass of particles impacting the wall. BH represents the Brinell hardness, F_s represents the particle shape coefficient, and u_p signifies the particle velocity.

3. CALCULATION VERIFICATION

3.1 Verification of Erosion Calculation

Experimental verification of erosion complements numerical calculations, validating the accuracy of the computational methodology. Therefore, we established an experimental system to investigate solid–liquid two-phase flows in a Y-type slurry valve, as depicted in Fig. 4(a). The pipeline experimental system was a complete close loop system and included a water storage tank, a stirrer, a regulating valve, a centrifugal pump, a motor, a flowmeter, and a Y-type slurry valve model. A 2/1.5B-AH series centrifugal slurry pump was employed for the conveyance of solid–liquid two-phase flows. The water storage tank was sized to hold up to 300 L and used to store a mixture of water and particles. The stirrer was formed by a combination of a motor and a rotating blade to ensure the particles were uniformly distributed in the

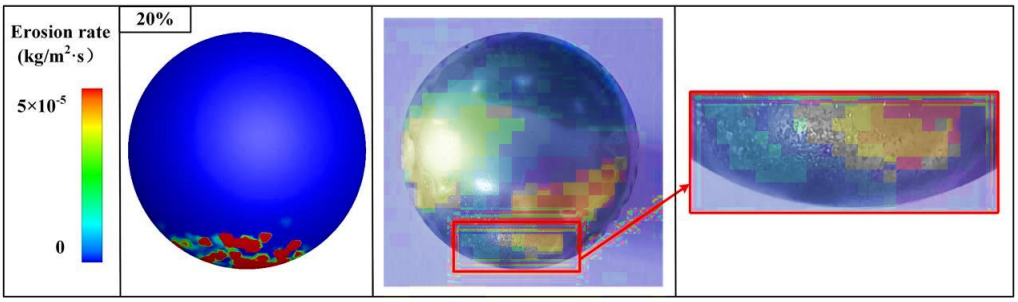

(a)

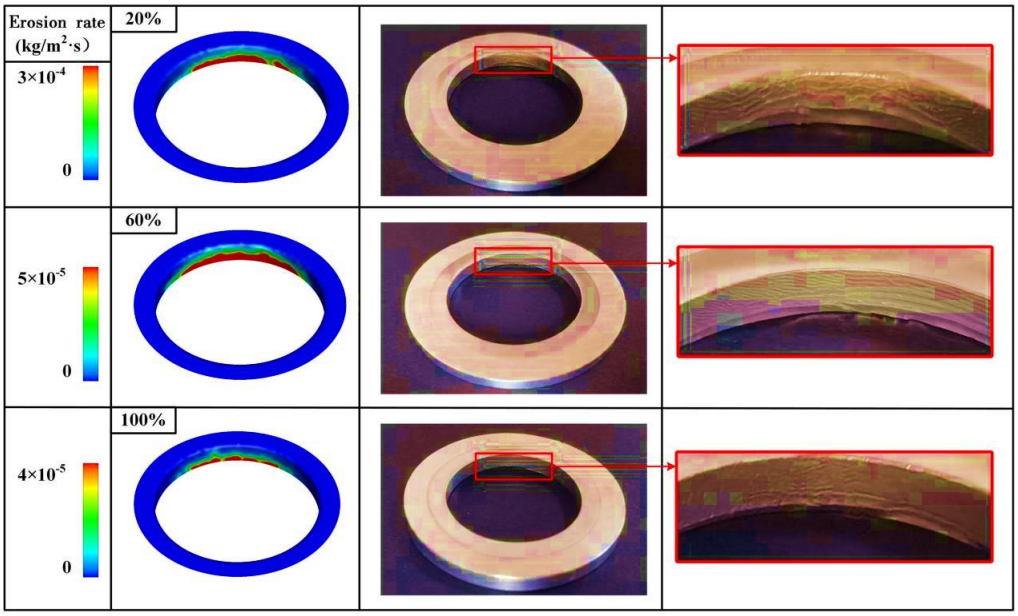

(b)

Fig. 5 Comparison and verification of numerical and experimental results

Table 1 Experimental conditions and related parameters

Name	Value
Inlet velocity	3m/s
Liquid phase and density	Water, 1000 kg/m3
Relative opening of the Y-type slurry valve	20%、60%、100%
Particle diameter	500μm
Particle material and density	Glass bead, 2600 kg/m3
Particle mass flow rate	0.39kg/s
Material of valve	Aluminum alloy

liquid flows, and we used a regulating valve to change the flow rate of the pipeline system. We used an LDG-SUP electromagnetic flow meter with a flow range of 2.26–22.6 m3/h that could withstand a maximum pressure of 4.0 MPa. An illustration of the experimental setup for examining solid–liquid two-phase flows in the Y-type slurry valve is depicted in Fig 4(b).

Note that we simplified the fabricated Y-type slurry valve for testing to make the experimental process more convenient, reduce the cost of modeling and calculation, and improve the accuracy of experiment and simulation. The Y-type slurry valve utilized in the experimental tests mirrored the structure employed in numerical simulations. We also designed the slurry valve so that the valve seat sealing ring could be disassembled, allowing us to change out the sealing ring for the different shapes under investigation. We also designed a fixed stroke for the valve stem in the valve body. The modulation of the Y-type slurry valve's relative opening was accomplished through the replacement of both the valve disc and valve stem components, and the three relative openings were designed to be 20%, 60%, and 100%. The particles employed in the experimental assessments comprised 500 μm glass beads characterized by a density of 2600 kg/m^3. Relevant experimental conditions and parameters are presented in Table 1.

The chosen erosion model's reliability in numerical calculations was affirmed through a comparative analysis between the numerical outcomes and experimental results. Figure 5(a) illustrates that when the relative opening was 20%, both numerical and experimental results yielded major erosion at the downward side of the positive valve disc surface, and we see good agreement in erosion distributions and positions between simulation and measurement. We also conducted erosion experimental tests on three valve opening degrees, and we compare the simulated valve seat seal ring erosion areas with the experimental results in Fig. 5(b). Numerical and

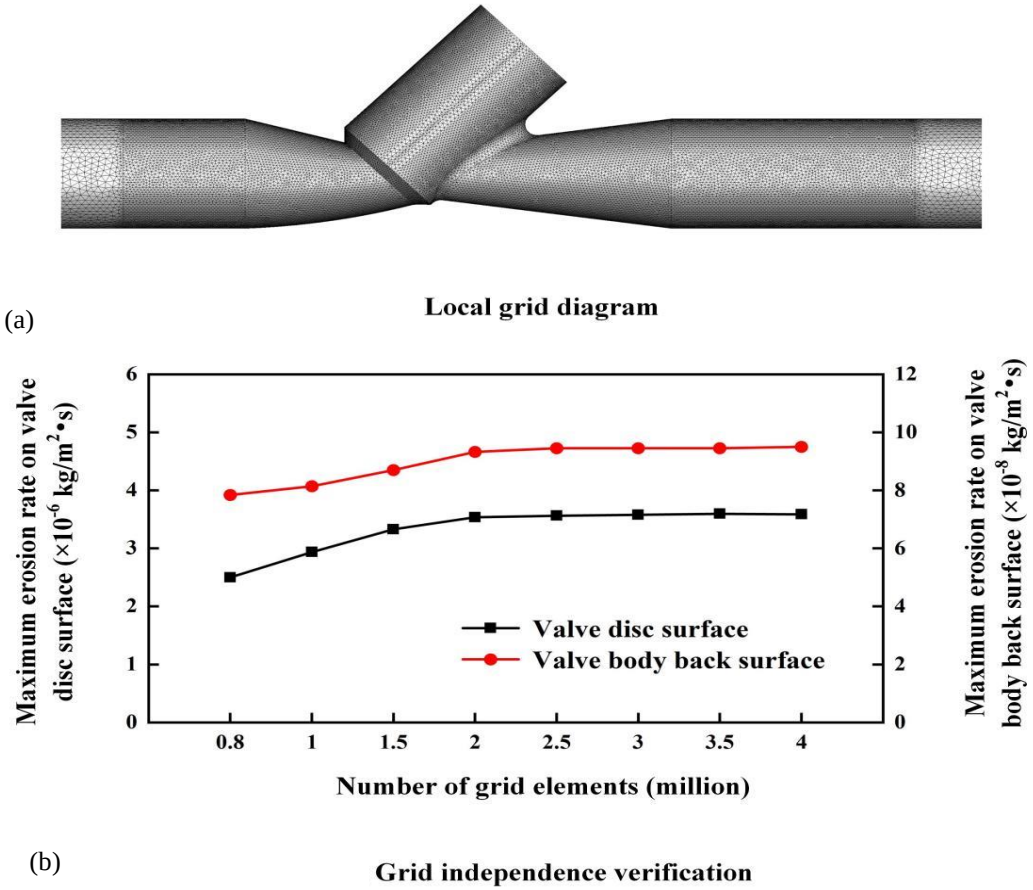

Fig. 6 Maximum erosion rates at different grid numbers

experimental observations revealed erosion concentrations along the lower edge of the inner side of the seal ring. The alignment between numerical erosion patterns and experimental findings underscores the precision of the erosion model employed in predicting particle erosion characteristics in Y-type slurry valves.

3.2 Grid Independence Study

Grid parameters have obvious effects on the precision of numerical simulations. Faster calculation speeds can be achieved with smaller numbers of grid elements, but this generally results in larger calculation error, negatively impacting the simulation accuracy. Larger numbers of grid elements can provide higher accuracy, but this will extend the calculation time and potentially waste computing resources. To obtain the appropriate grid number, we conducted a grid independence study, and we investigated the maximum disc and valve body back surface erosion rates with different grid numbers. We set the number of numerical grid elements to 0.8, 1, 1.5, 2, 2.5, 3, 3.5, and 4 million, and a representation of the local grid is shown in Fig. 6(a). Figure 6(b) distinctly illustrates that, beyond 2 million numerical grid elements, augmenting the grid count has marginal influence on the maximum erosion rates for both components. Therefore, we selected a numerical grid element count of 2 million for simulating particle–liquid two-phase flows in the valve.

3.3 Division of Main Erosion Areas

The seat sealing ring is an important component in Y-type slurry valves, and changing the shape of valve seat sealing ring will directly affect the movement state of particles in the flow field, leading to changes in the erosion characteristics in the valve. As illustrated in Fig. 7, prior investigations have underscored that predominant erosion regions in valves and pipelines encompass the posterior wall of the valve body, the internal surface of the valve seat, the downstream pipeline, and the frontal surface of the valve disc. In this investigation, a comprehensive numerical analysis was conducted to scrutinize erosion distributions and rates within these specified regions of the valve.

3.4 Boundary Conditions

We employed a CFD-DEM approach utilizing the Euler–Lagrange method for resolving the two-phase flow field. Zhang's semi-empirical erosion model was employed for calculating erosion rates, while numerical computations were conducted using the realizable k-ε model. This paper assumes the incompressibility of the liquid phase. The model prescribes a velocity inlet for the inlet condition and designates a pressure outlet for the outlet condition. The solid and liquid phases were completely mixed into the computational domain, and the initial velocities of particles and fluids remained the same. We also set a non-slip wall surface on the valve wall, and

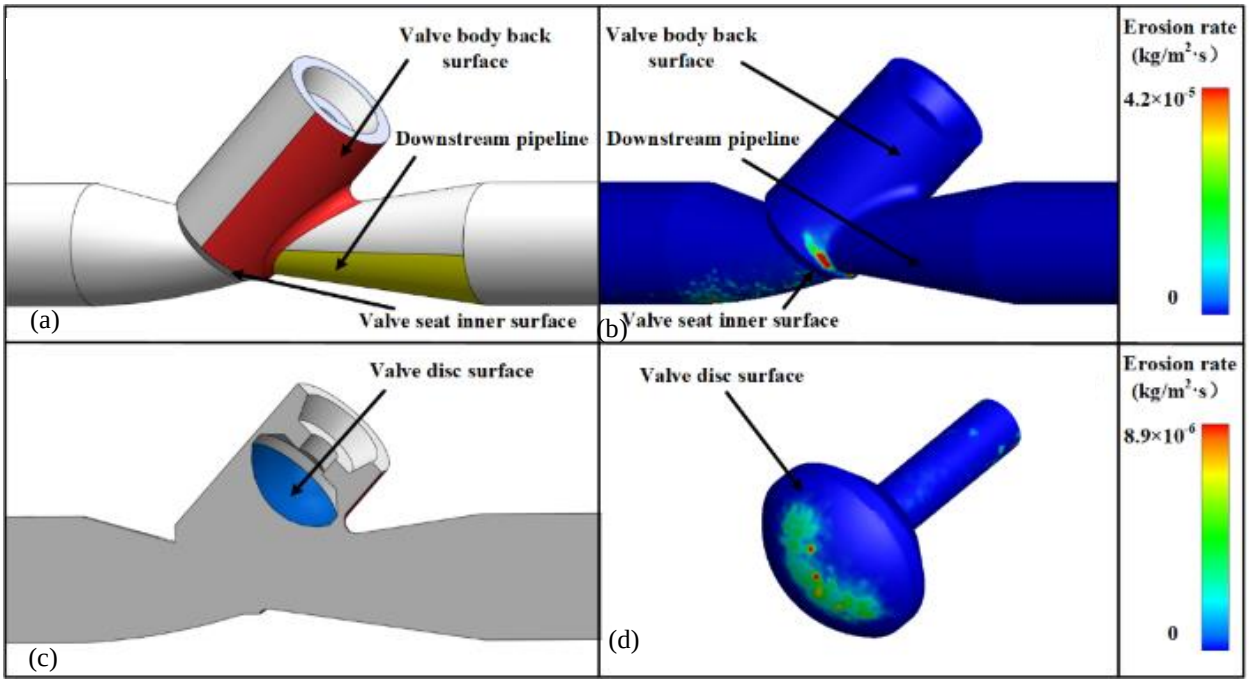

Fig. 7 Division of main erosion areas in Y-type slurry valve

Table 2 Numerical simulation parameters

Name	Value
Liquid phase and density	Water, 1000 kg/m3
Input speed	3m/s
Relative opening of the Y-type slurry valve	20%、40、60%、80、100%
Particle diameter	50μm、250μm
Particle material and density	Glass bead, 2600 kg/m3
Particle mass flow rate	1.8kg/s

the relevant numerical simulation parameters are shown in Table 2.

4. RESULTS AND DISCUSSION

4.1 Characteristics of Solid-Liquid Two-Phase Flows

4.1.1 Velocity and Pressure Distribution

We investigated the influence of different inner angles in the valve seat configuration on velocity and pressure distributions. Figure 8 illustrates the velocity and pressure distributions of the liquid phase under various valve seat shapes, with a particle diameter of 50 μm within the valve. The simulation results demonstrate a noticeable increase in the width of the high-speed jet zone as the valve opening angle rises. Additionally, when the fluid entered the valve body, the sealing ring provided the fluid with an inclined upper wall path. This led to the high-speed fluid entering the downstream pipeline at a particular inclination angle, altering the wake of the high-speed jet with an upward deflection. Moreover, with the sealing ring shape transitioning from 45° to 90°, a notable alteration in the pressure distribution within the flow field occurred. Concomitantly, there was a gradual elevation in the pressure within the cavity above the valve disc.

Figure 9 illustrates the flow velocity and pressure patterns of the liquid phase under varying valve seat shapes, employing a particle diameter of 250 μm. With an elevation in the inner angle of the valve seat sealing ring, the high-speed jet belt exhibited a reduced length, coupled with a gradual upward shift of the wake. Simultaneously, the heightened inner angle induced a more pronounced deformation of the high-speed jet belt, amplifying its impact on pressure distributions and particle motion patterns. The inner angle of the valve seat sealing ring predominantly influenced pressure distributions in the cavity above the valve disc, resulting in a gradual increase in pressure as the inner angle rose.

4.1.2 Valve Flow Performance

The flow coefficient serves as a crucial parameter for characterizing the performance of the valve. Variations in seat sealing ring shapes induce alterations in the flow channel structure, leading to modifications in the valve's flow coefficient and capacity. The flow coefficient can be expressed mathematically as

$$K_v = q_v \sqrt{\frac{\rho}{\Delta P}} \tag{8}$$

where ΔP represents the pressure difference across the valve, measured in Pascals (Pa), q_v denotes the volume flow rate expressed in cubic meters per hour (m^3/h), and ρ signifies the fluid density in kilograms per cubic meter (kg/m^3).

We investigated the impact of four distinct seat shapes on the flow capacity of a Y-type slurry valve under valve opening degrees of 20%, 60%, and 100% with a particle diameter of 250 μm, as shown in Fig. 10. At a valve opening degree of 20%, a valve seat sealing ring angle of 45° yielded the maximum flow coefficient of 75.2. At the valve opening of 60%, variation in the shape of the valve

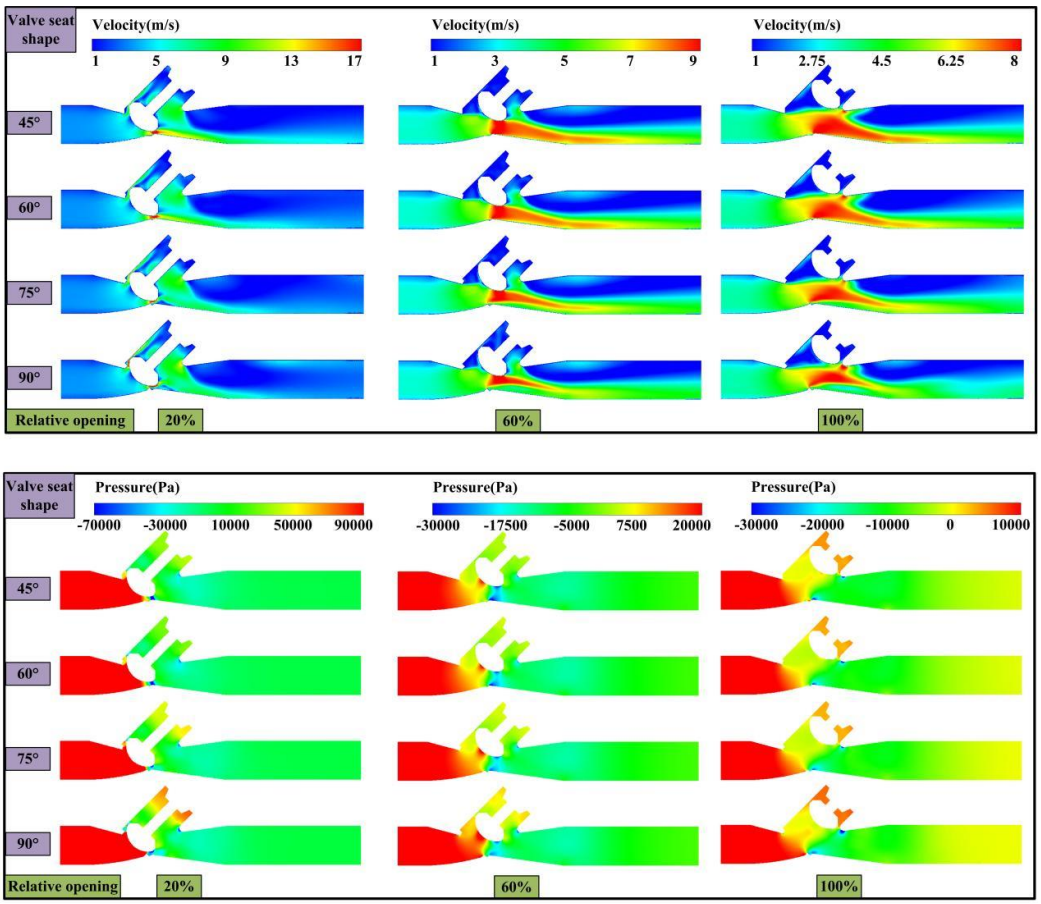

Fig. 8 Velocity and pressure distributions at different seat structures (d =50μm)

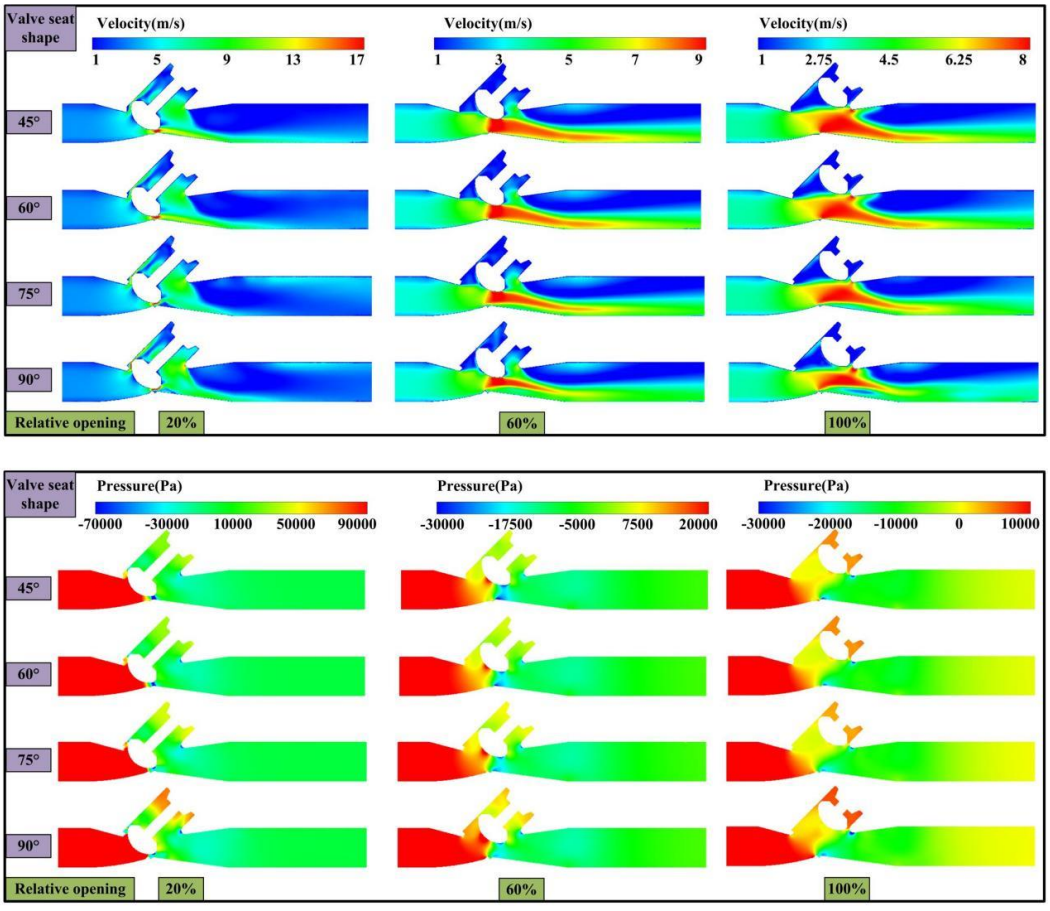

Fig. 9 Velocity and pressure distributions at different seat structures (d=250μm)

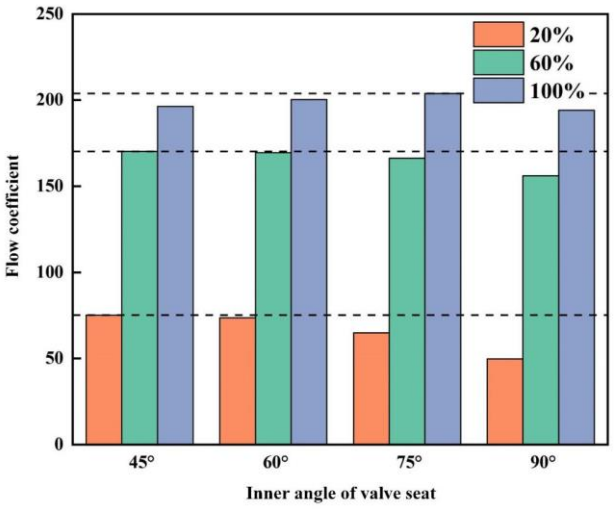

Fig. 10 Flow coefficients of T-type slurry valve at different seat structures

seat sealing ring had little effect on the flow coefficient. At a sealing ring angle of 45°, the valve exhibits its maximum flow coefficient, reaching a value of 169.5. With increases in the valve seat sealing ring inner angle, the flow coefficient gradually decreased at valve opening degrees of 20% and 60%. However, the flow coefficient increased with increases in the valve seat sealing ring inner angle at an opening degree of 100%, and the valve achieved the best performance with a valve seat sealing ring inner angle of 75°.

4.1.3 Particle Velocity Distribution

The study of particle distribution is an effective method to analyze the characteristics of two-phase flows, and the accumulation of particles near the main wall and high-speed particle flows will impact erosion characteristics in the valve. Therefore, we investigated particle distribution and motion with particle diameters of 50 and 250 μm and valve opening degrees of 20%, 60%, and 100%.

Figure 11 shows particle velocity distributions for the four different valve seat sealing ring shapes at a particle diameter of 50 μm and a relatively uniform particle distribution. At smaller valve opening degrees, the number of particles below the initial position where the valve seat connected with the downstream pipeline decreased. When the valve opening degree was small, the particle distribution in the entire valve flow channel was relatively uniform and concentrated on the right side inside the valve body. The particle velocity was also relatively high in this scenario. As the valve seat sealing ring inner angle increased, the cross-sectional area of the flow channel diminished, leading to heightened velocities of both the liquid and particle phases. This resulted in an increased force transmitted by the liquid phase to the particles, leading to an elevation in particle velocities.

With a valve seat sealing ring inner angle of 90°, there was clearly a significant low-velocity region at the downward side of the initial position where the valve seat connected to the downstream pipeline. With increases in the valve seat sealing ring inner angle, the size of the flow region with low velocity increased, and particles near this region followed the high-speed jet to move downstream. In addition, there were fewer particles in the low-velocity region.

Figure 12 shows the particle velocity distributions for the four different valve seat sealing ring shapes at a particle diameter of 250 μm with particles deposited at the downward side of the pipeline due to gravity. At an innerangle of 90° for the valve seat sealing ring, particles proximate to the valve disc experienced enhanced kinetic energy transmission attributable to the heightened liquid phase velocity. Consequently, the particle velocity near the valve disc exhibited a relatively elevated magnitude. At a reduced inner angle of the valve seat sealing ring, a zone characterized by a diminished particle count was

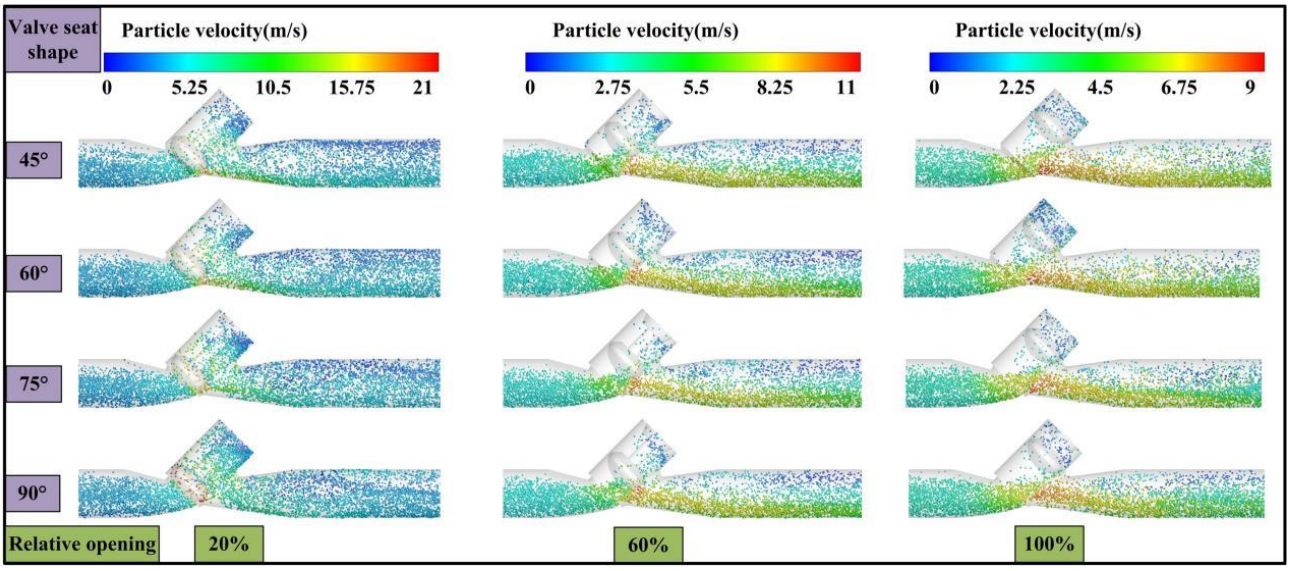

Fig. 11 Particle velocity distributions at different seat structures (d=50μm)

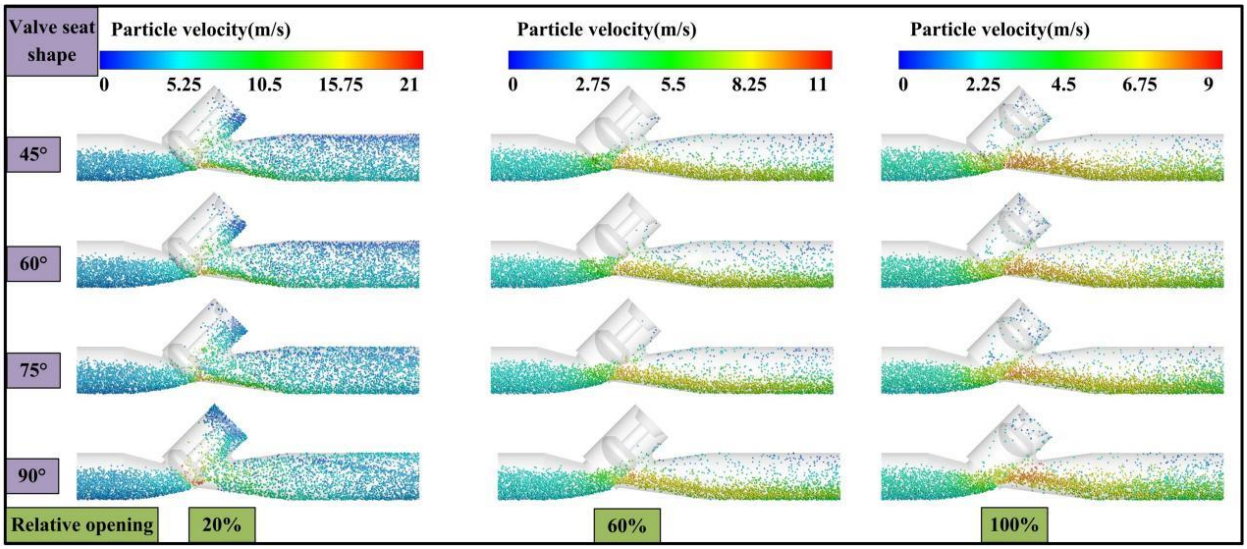

Fig. 12 Particle velocity distributions at different seat structures (d=250μm)

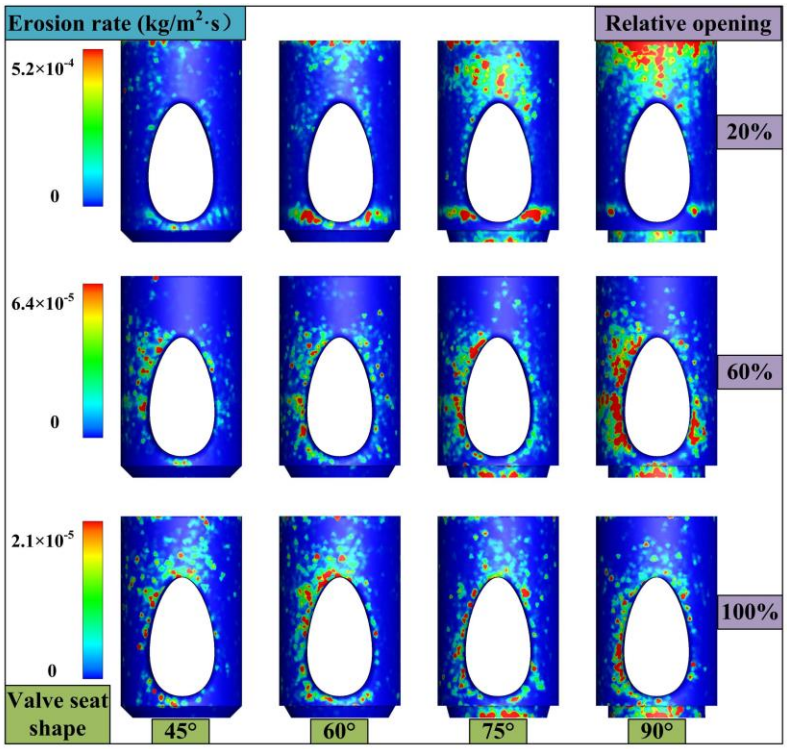

Fig. 13 Erosion distributions on back wall of valve body and valve seat (d=50μm)

observed beneath the primary particle–liquid flows. This behavior was identical to the low-speed region with recirculating flows beneath the high-speed jet belt. In valves with a reduced valve seat sealing ring angle, particles moved near the downward side wall of the downstream pipeline, while those with a larger angle maintained a distance from the wall.

4.2 Erosion on Back Wall of Valve Body and Valve Seat

We also analyzed the erosion distributions on the back wall of the valve body and the valve seat with the four different valve seat sealing ring shapes. The predominant factor leading to wall erosion was identified as the high-frequency collisions between particles and the surface of the wall. For consistency in our analysis, we investigated the erosion characteristics on the posterior surface of the valve body and the valve seat at particle diameters of 50 and 250 μm.

Figure 13 illustrates the erosion distributions on the posterior surface of the valve body and the valve seat with the four different valve seat sealing ring shapes and a particle diameter of 50 μm. From the plots in Fig. 13, it is clear that the rare surface of the valve body exhibited more dispersed erosion with spot-like patterns. With an increase in the valve seat sealing ring inner angle, the erosion distribution area gradually increased. When the valve seat sealing ring inner angle increased with a 20% opening, the particle concentration in the upper section of the valve body cavity exhibited an increment, leading to an increase in the number of collisions with the wall surface and more severe erosion on the posterior surface of the valve body.

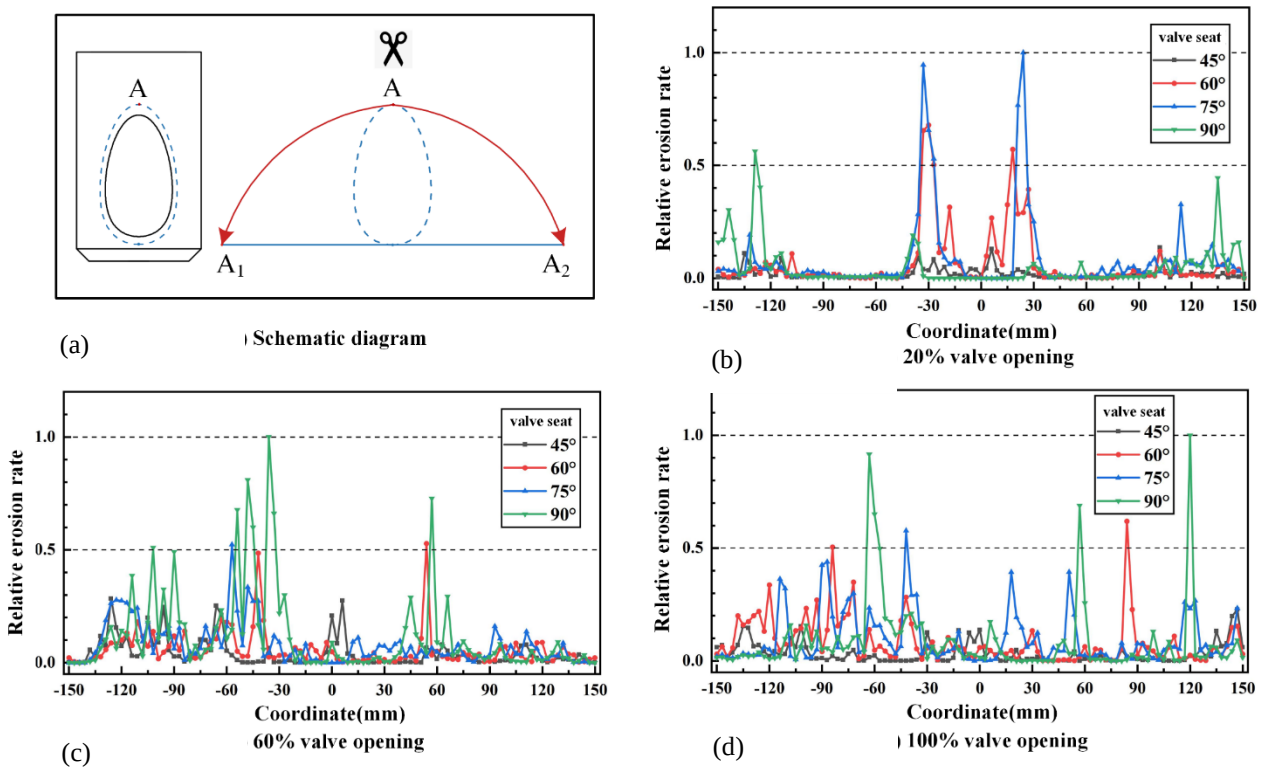

Fig. 14 Relative erosion rates of back wall of valve body (d= 50μm)

When the valve seat sealing ring inner angle was 90°, we observed a larger number of particles above the valve disc that were more evenly distributed, resulting in serious erosion on the upper region of the valve body's back wall. With valve openings of 60% and 100%, an augmentation in the inner angle of the valve seat sealing ring led to a more extensive erosion area on the posterior surface of the valve body. Erosion was primarily concentrated near the junction of the valve body's rear wall and the downstream pipeline.

With respect to the valve seat, we observed almost no erosion on the valve seat with valve seat seal ring inner angles of 45° and 60°. However, we did observe erosion with angles of 75° and 90°. With these seal angles, the collision and rebound angles between the particle flow direction and the inner surface of the valve seat exhibited an augmentation with increased particle velocity. Therefore, the collision and rebound were more intense, leading to more serious erosion on the valve seat.

Figure 14 illustrates the comparative erosion rates on the posterior surface of the valve body for the four different valve seat sealing ring shapes. For this analysis, we extracted the relative erosion rates along the blue dashed line encircling the annular region near the connection point of the valve body., as shown in the upper left figure of Fig. 14. This line was configured at a uniform distance of 6 mm from the connection point between the valve body and the downstream pipeline. Assuming a cut at point A, the dotted line extends on both sides, forming the blue band A1-A2. With 20% valve opening, larger erosion rates were generated on the posterior surface of the valve body with valve seat sealing ring inner angles of 60° and 75°, and as expected, symmetrical peaks were identified on either side of the center point, delineating two high-erosion areas within the annular region of the posterior surface of the valve body. As particles entered the downstream pipeline, their velocities were notably higher compared to cases with smaller valve seat sealing ring angles, and the high-velocity particles experienced intensified collisions with the wall surface, resulting in heightened erosion on the back wall. When the sealing ring inner angle was 90°, a substantial particle accumulation occurred in the cavity above the valve disc, leading to a reduction in the relative erosion rates within the annular region on the posterior surface of the valve body. With valve openings of 60% and 100%, the erosion rates on the back wall were largest when the valve seat sealing ring inner angle was 90°, and the erosion rates exhibited a scattered and irregular distribution within the annular area on the posterior surface of the valve body.

Figure 15 illustrates the comparative erosion rates of the valve seat with four distinct valve seat sealing ring shapes. To intuitively understand the erosion rates for different valve seat designs, we extracted and analyzed the comparative erosion rates along the central axis of the valve seat. This line is shown as the line segment B1B2 in the upper left figure in Fig. 15. The erosion was primarily distributed on the valve seat for valve seat sealing ring inner angles of 75° and 90°, and the overall valve seat erosion rates were higher with larger inner angles. The erosion rates were symmetrically distributed, and the erosion rate was similar with inner angles of 75° and 90°. The valve seat sealing rings with larger inner angles changed the local structure of the flow channel. This changed the trajectory of particles and led to more intense collisions and impacts of the high-speed jet flows on the valve seat, resulting in more severe erosion.

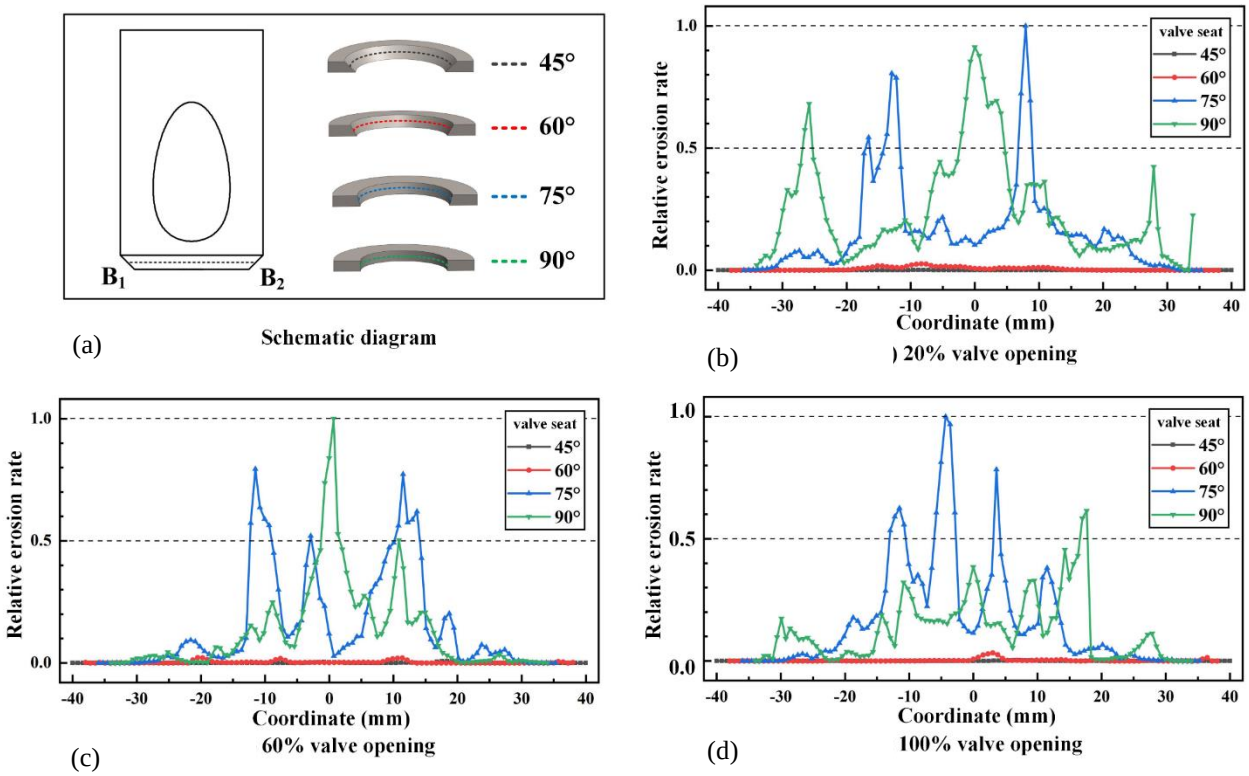

Fig. 15 Relative erosion rates of inner surface of valve seat (d= 50μm)

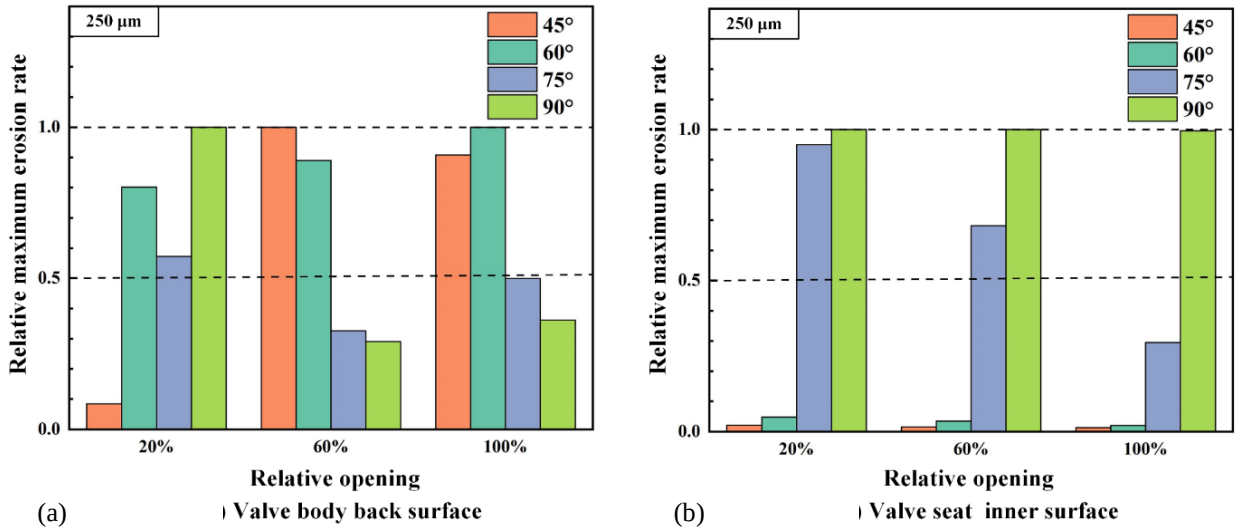

Fig. 16 Maximum relative erosion rates of back wall of valve body and valve seat (d=50μm)

Figure 16 illustrates the peak comparative erosion rates on the posterior surface of the valve body and the valve seat across the four distinct valve seat sealing ring shapes. With 20% valve opening, the highest comparative erosion rates for both the posterior surface and the valve seat were identified at a valve seat sealing ring inner angle of 75°. With a 60% valve opening, the maximum relative erosion rates of both structures were observed at a valve seat sealing ring inner angle of 90°. With 100% valve opening, the peak relative erosion rate on the back wall occurred at a valve seat sealing ring inner angle of 90°, whereas the maximum relative erosion rate on the valve seat was noted at a valve seat sealing ring inner angle of 75°. It is clear from this data that the maximum relative erosion rates occurred for larger inner angles.

Figure 17 depicts erosion patterns on the posterior surface of the valve body and the valve seat with the four different valve seat sealing ring shapes and a particle diameter of 250 μm. The comparative erosion rates on both the posterior surface of the valve body and the valve seat exhibited higher magnitudes when the particle diameter was 250 μm, in contrast to the erosion rates observed with a particle diameter of 50 μm. Symmetrically distributed erosion areas were observed on the posterior surface of the valve body. As the valve opening expanded,

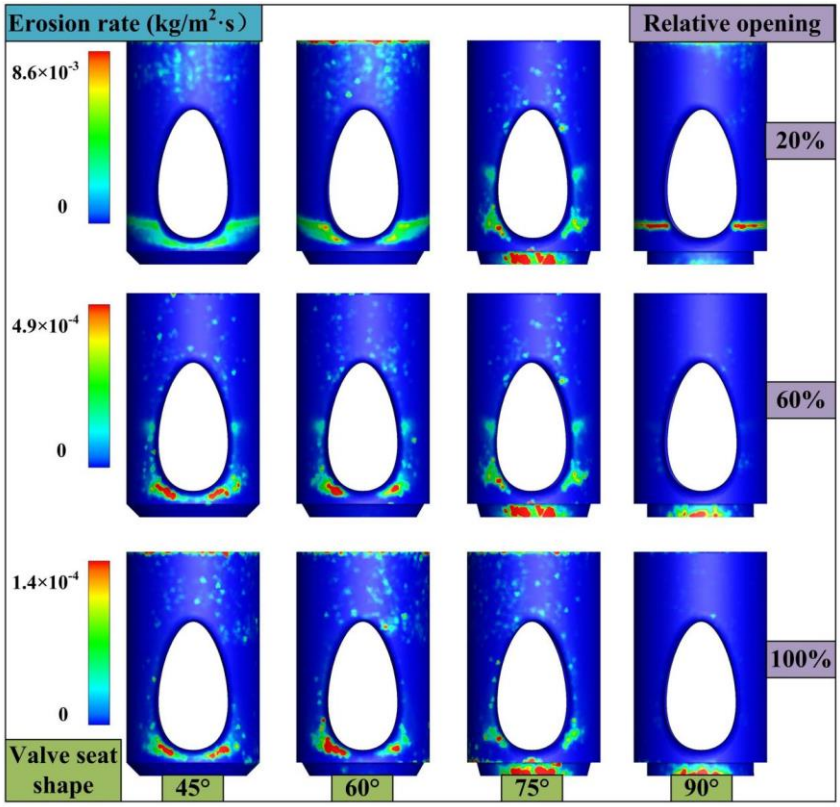

Fig. 17 Erosion distributions on back wall of valve body and valve seat (d=250μm)

the primary erosion area exhibited a gradual reduction. The erosion rate also gradually decreased due to the blocking effect of the valve disc at smaller valve openings. As the inner angle of the valve seat sealing ring increased, the erosion distributions progressively concentrated in specific localized regions. With a valve opening of 20%, the predominant erosion zone on the back wall exhibits a symmetrical pattern, concentrated in the central and downward regions, particularly evident with a valve seat sealing ring inner angle of 45°. With an increase in the inner angle of the valve seat sealing ring, local high-erosion areas appeared on the back wall, and a slender erosion strip area appeared at the position corresponding to the valve disc with a valve seat sealing ring inner angle of 90°.

Regarding the valve seat, the inclination angle between its inner surface and the trajectory of particle movement was relatively modest, and as a result, there was almost no erosion on the valve seat for inner angles of 45° and 60°. However, as the inner angles increased to 75° and 90°, the change in the shape of the flow channel impacted the trajectory of particles, and the main particle collision area was transferred from the back wall to the middle of the valve disc. This led to a local large-erosion area symmetrically distributed in the center of the valve seat.

Figure 18 illustrates the comparative erosion rates on the posterior surface of the valve body corresponding to the four distinct shapes of valve seat sealing rings. The erosive impact on the valve body's back wall predominantly localized within the annular region encircling the junction between the valve body's back wall and the downstream pipeline. With a particle diameter of 250 μm, the erosion rate distributions were symmetrical in an M-shaped pattern, and at each valve opening level, the erosion rate in the vicinity of the central point exhibited a comparatively subdued level, featuring two symmetrical peaks on opposing sides. With 20% valve opening, the erosion rates were significantly higher at valve seat sealing ring inner angles of 60°, 75°, and 90°, exhibiting two prominent, symmetrical erosion zones within the annular region of the back wall. As the valve seat sealing ring inner angle increased, the erosion rates gradually increased, and the peaks of the erosion rates moved farther from the center point. With valve openings of 60% and 100%, the erosion rates on the back wall were larger at inner angles of 45° and 60°. This was because the flow channel changed the trajectory of particles with larger valve openings and smaller inner angles, and more particles collided with the back wall, leading to larger relative erosion rates.

Figure 19 illustrates the comparative erosion rates of the valve seat with a particle diameter of 250 μm. In this case, erosion rates were larger at the valve seat sealing ring inner angles of 75° and 90°, while there was almost no erosion on the valve seat with smaller inner angles. Note that this is also apparent from the data in Fig. 16. The relative erosion rates of the valve seat were symmetrically distributed at different valve opening levels, and the erosion rates were much larger an inner angle of 90° compared with those at an inner angle of 75°. The valve seat sealing ring with larger inner angles changed the area of the flow channel as well as the direction of particle motion. This resulted in increased particle deposition in the central and lower regions of the flow channel, exerting a greater impact on the valve seat and, consequently, causing more pronounced erosion on the valve seat at an inner angle of 90°.

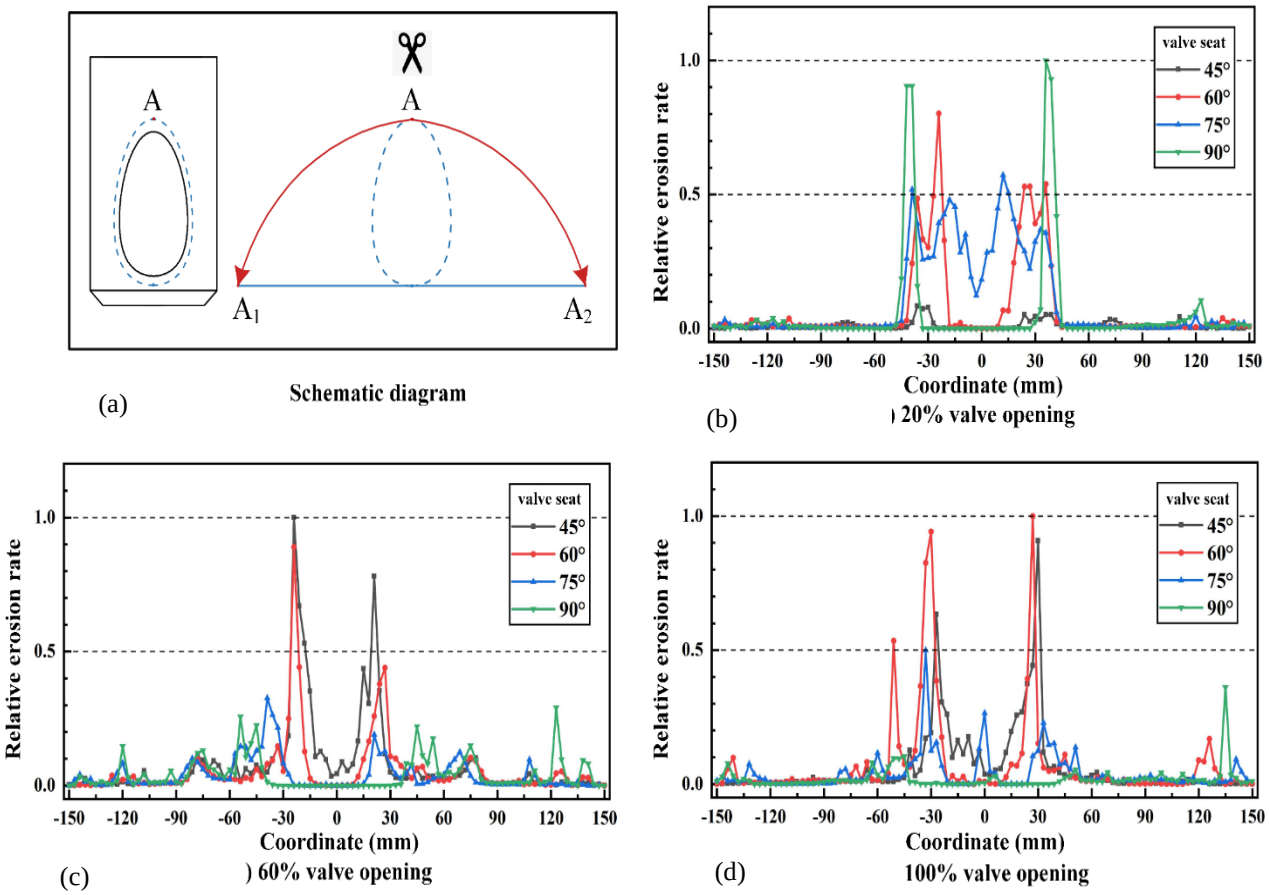

Fig. 18 Relative erosion rates of back wall of valve body (d=250μm)

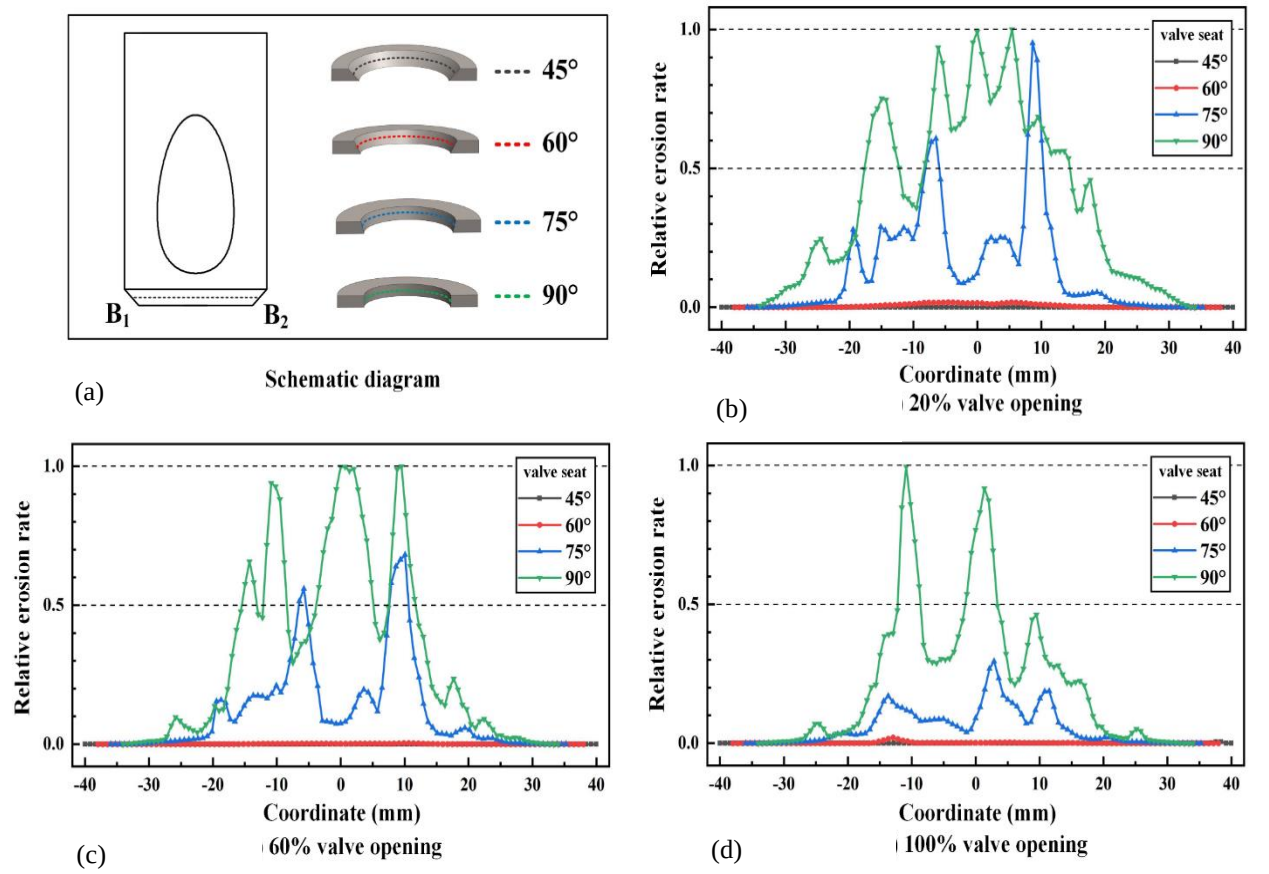

Fig. 19 Relative erosion rates of inner surface of valve seat (d=250μm)

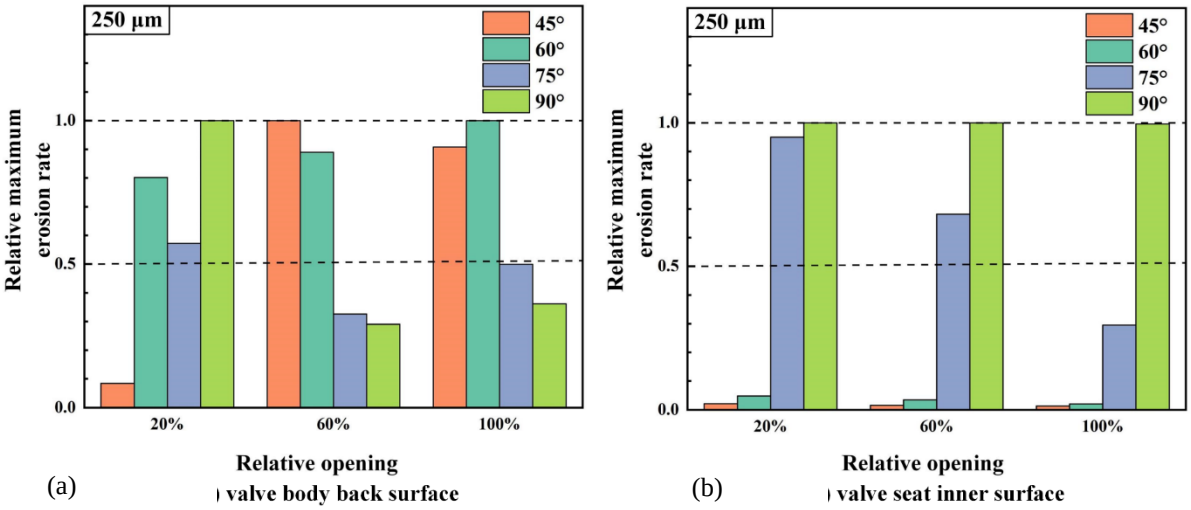

Fig. 20 Maximum relative erosion rates of back wall of valve body and valve seat (d=250μm)

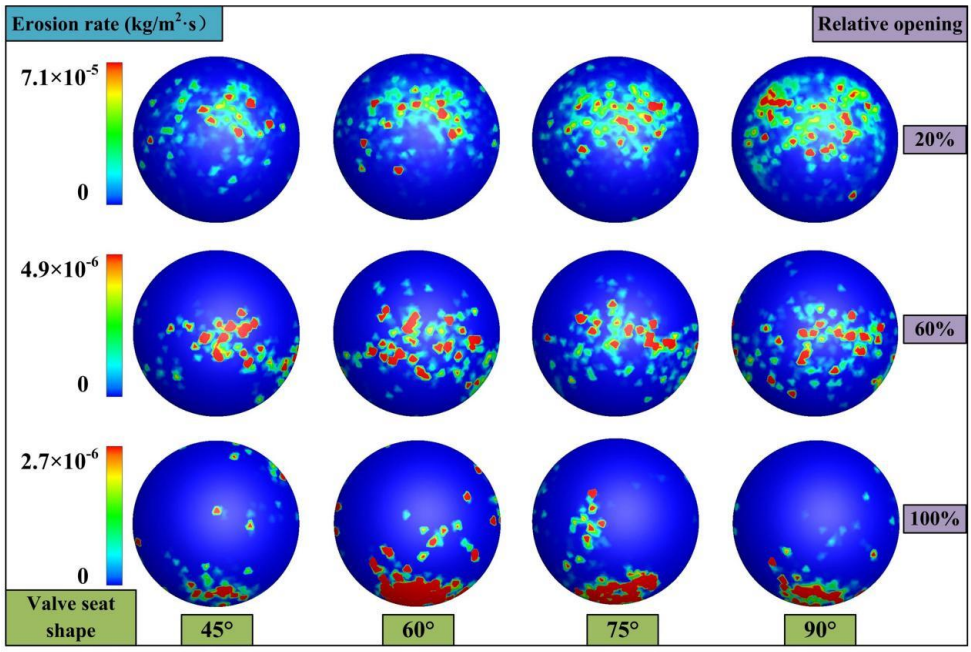

Fig. 21 Erosion distribution on the positive surface of valve disc (d=50μm)

Figure 20 illustrates the maximum comparative erosion rates observed on both the posterior surface of the valve body and the valve seat for the four different valve seat sealing ring shapes. With 20% valve opening, the maximum relative erosion rate was observed at a valve seat sealing ring inner angle of 90°. With 60% valve opening, the maximum relative erosion rate was observed at a valve seat sealing ring inner angle of 45°. However, with 100% valve opening, the maximum relative erosion rate was observed at a valve seat sealing ring inner angle of 60°. At larger valve opening levels and sealing ring inner angles, the maximum relative erosion rates on the back wall were smaller. This is attributed to alterations in the flow channel configuration between the valve disc and the valve body, resulting in a reduced incidence of particle impact on the posterior surface of the valve body. For the valve seat, the maximum relative erosion rates were much higher at larger inner angles. In contrast to the peak relative erosion rates on the back wall, alterations in the flow channel between the valve disc and the valve seat occurred as a result of variations in the valve opening extent and the inner angle of the valve seat sealing ring. This led to more particles colliding with the valve seat and more severe erosion on the valve seat at larger inner angles.

4.3 Erosion of Positive Surface of Valve Disc

Erosion on the positive surface of the valve disc poses a threat to the sealing efficacy of Y-type slurry valves. Such erosion adversely impacts the valve's regulatory capabilities and may result in leakage within the pipeline transportation system. To comprehend erosion patterns on the valve disc, we scrutinized the erosion characteristics on the positive surface of the valve disc under various valve seat sealing ring shapes and levels of valve opening, as detailed previously.

Figure 21 shows erosion patterns on the positive surface of the valve disc at different valve seat sealing ring inner angles with a particle diameter of 50 μm. With a valve opening of 20%, the predominant erosion region on the positive surface of the valve disc was situated on the

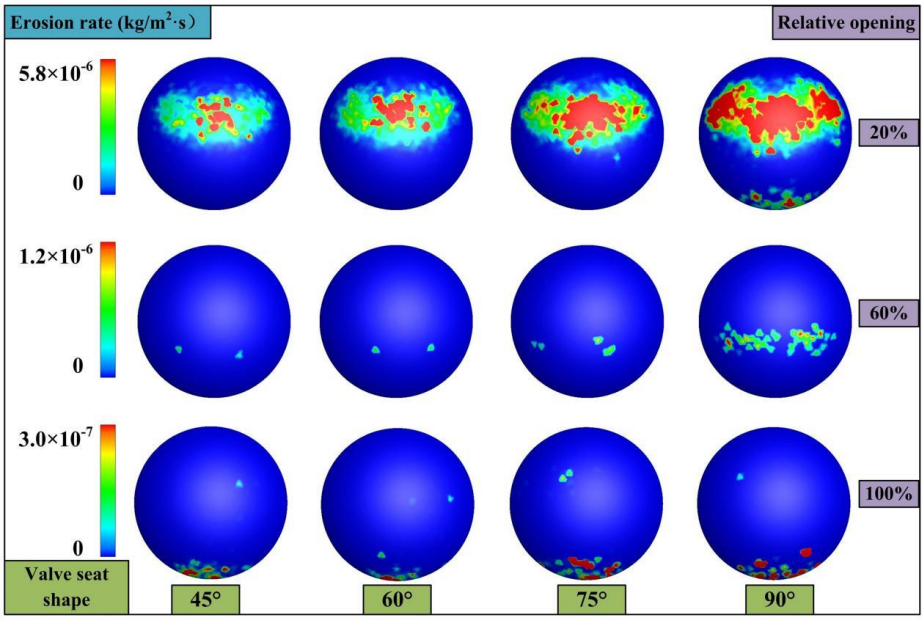

Fig. 22 Erosion distribution on the positive surface of valve disc (d=250μm)

upper side of the disc. As the valve opening increased, the primary erosion region shifted towards the lower side of the disc and gradually diminished, and the erosion rate also decreased. At a 60% valve opening, the primary erosion region on the positive surface of the disc was predominantly oriented towards the lower side of the disc. With an increase in the valve seat sealing ring inner angle, the predominant erosion zone on the positive surface of the disc exhibited a gradual expansion. and the erosion was more widely dispersed. This is because the 50-μm particles had good tracking ability with the liquid phase, and more particles moved into the valve cavity with a uniform distribution. At a 20% valve opening and an increased valve seat sealing ring inner angle, the flow area between the valve disc and the seat experienced a reduction, and the blocking effect of the valve disc caused more particles to be aggregated and collide with the positive surface of the valve disc. This resulted in an expansion of the erosion zone on the positive surface of the valve disc.

Figure 22 illustrates erosion patterns on the positive surface of the valve disc, considering four distinct inner angles of the valve seat sealing ring and a particle diameter of 250 μm. Similar to the erosion patterns observed on the positive surface of the valve disc with 50-μm particles, the principal erosion zone shifted towards the lower side of the valve disc and progressively decreased with the rise in the valve opening degree. In addition, for lower valve opening levels, the principal erosion region exhibited symmetrical distribution on the valve disc and was considerably more extensive. The primary erosion region on the positive surface of the valve disc exhibited a gradual enlargement in conjunction with the escalation of the valve seat sealing ring. The primary erosion zone exhibited reduced dimensions at higher valve opening levels and smaller inner angles, attributed to the diminished particle impact on the positive surface of the valve disc under these conditions. Compared with erosion distributions with 50-μm particles, the main erosion area was larger at 20% valve openings and smaller at 60% and 100% valve openings. In addition, the erosion rate was smaller for 250-μm particles than it was for 50-μm particles. The reason for this is that at the same mass flow rate, more particles were initialized and moved into the valve cavity, causing a higher number and rate of collisions with the positive surface of the valve disc. These additional collisions led to higher erosion rates on the positive surface of the valve disc for the smaller particles.

5. CONCLUSION

In this investigation, we conducted numerical simulations to explore the features of particle–liquid two-phase flows and particle erosion in Y-type slurry valves, considering various valve seat sealing ring shapes, valve opening levels, and particle diameters. To control the trajectory of particles and inhibit erosion on the main components of Y-type slurry valves, we designed four variations of valve seat sealing rings with different inner angles. The structure of the valve seat sealing ring was observed to have obvious effects on the characteristics of particle–liquid two-phase flows. With an elevation in the inner angle of the valve seat sealing ring, the high-speed jet region between the valve disc and the valve seat exhibited a gradual shift towards the lower side of the downstream pipeline, subsequent to the valve disc. Concurrently, there was a progressive rise in pressure within the valve cavity. Changes in the valve seat sealing ring inner angle caused changes in the valve flow channels and these flow channel changes modified the trajectory of particles through the valve. As the inner angle of the valve seat sealing ring increased, a reduction in particle concentration was observed on the lower side of the flow channel between the valve seat and the downstream pipeline.

These changes in particle trajectories modified erosion distributions and rates on the main components of

the valve, such as the posterior surface of the valve body, the valve seat, and the positive surface of the valve disc. For 50-μm particles, the erosion distributions on the posterior surface of the valve body were more dispersed in dot-like patterns, while the erosion distributions took the form of flakes or thin strips for 250-μm particles. For smaller particle diameters, the main erosion areas and relative erosion rates gradually increased with increases in the valve seat sealing ring inner angle. However, the main erosion areas and relative erosion rates decreased with increases in the valve seat sealing ring inner angle for 250-μm particles. This result was due to the combined effects of particle number and flow channel. For equivalent mass flow rates, a notable decrease in particle count is evident with larger particle diameters. In addition, alterations in the flow channel between the valve disc and the valve body ensued with variations in the inner angle of the valve seat sealing ring, leading to different collision behaviors on the posterior surface of the valve body. With respect to the valve seat, the predominant erosion region became more concentrated at the center of the valve seat with increases in the valve seat sealing ring inner angle. The main erosion areas and relative erosion rates of the valve seat were much larger at larger inner angles compared with those at smaller inner angles. With respect to the valve disc, the erosion area and the comparative erosion rate of the positive surface of the valve disc increased as the valve seat sealing ring inner angle increased.

ACKNOWLEDGEMENTS

This research was funded by National Natural Science Foundation of China (Granted No.52222601 and 52006198), Key Research and Development Program of Zhejiang Province (Granted No. 2023C01171 and 2023C01172) and Zhejiang Sci-Tech University .

CONFLICT OF INTEREST

No conflict of interest exits in the submission of this manuscript, and manuscript is approved by all authors for publication. I would like to declare on behalf of my co-authors that the work described was original research that has not been published previously, and not under consideration for publication elsewhere, in whole or in part. All the authors listed have approved the manuscript that is enclosed.

AUTHORS CONTRIBUTION

Guang Zhang: Writing-Original draft, Reviewing and Editing, Resources, Funding acquisition. **Yihao Zhang:** Conceptualization, Methodology, Writing-Original draft preparation. **Jialin Xin:** Conceptualization, Writing-Original draft, Writing Reviewing and Editing. **Desheng Chen:** Formal analysis, Writing-Reviewing and Editing, Funding acquisition. **Zhe Lin:** Formal analysis, Writing-Reviewing and Editing, Funding acquisition.

REFERENCES

Auton, T., Hunt, J., & Prud'Homme, M. (1988). The force exerted on a body in inviscid unsteady non-uniform rotational flow. *Journal of Fluid Mechanics, 197*, 241-257. https://doi.org/10.1017/S0022112088003246

Barati, R., Salehi Neyshabouri, S. A. A., & Ahmadi, G. (2014). Development of empirical models with high accuracy for estimation of drag coefficient of flow around a smooth sphere: An evolutionary approach. *Powder Technology, 257*, 11-19. https://doi.org/10.1016/j.powtec.2014.02.045.

Chen, Y., Xiong, H., Cheng, H., Yu, C., & Xie, J. (2020). Effect of particle motion on the hydraulic collection of coarse spherical particles. *Acta Mechanica Sinica*, *36*(1), 72-81. http://doi.org/10.1007/s10409-019-00922-6

Costa, A., & Nara, R. (2020). Computational fluid dynamics erosion investigation using single objective adjoint shape optimization. *Journal of Pipeline Systems Engineering and Practice*, *11*, 6020001. http://doi.org/10.1061/(ASCE)PS.1949-1204.0000468

Dumitrache, C. L., & Hnatiuc, B. (2018). Comparative CFD analysis of naval plug valve. *Journal of Physics. Conference Series*, *1122*(1), 12012. http://doi.org/10.1088/1742-6596/1122/1/012012

Gopaliya, M. K., & Kaushal, D. R. (2022). Numerical prediction of solid-liquid slurry flows and derivation of simulation-based correlations for local solid concentration. *Progress in Computational Fluid Dynamics, an International Journal*, *22*(5), 303-316. http://doi.org/10.1504/PCFD.2022.125736

Grant, G., & Tabakoff, W. (1975). Erosion prediction in turbomachinery resulting from environmental solid particles. *Journal of Aircraft, 12*(5), 471-478. http://doi.org/10.2514/3.59826

Greitzer, E., Tan, C., & Graf, M. (2004). *Internal Flow: Concepts and Applications*. https://doi.org/10.1017/CBO9780511616709

Gu, D., Cheng, C., Liu, Z., & Wang, Y. (2019). Numerical simulation of solid-liquid mixing characteristics in a stirred tank with fractal impellers. *Advanced Powder Technology, 30*(10), 2126-2138. http://doi.org/10.1016/j.apt.2019.06.028

Lai, F., Wang, Y., EI-Shahat, S. A., Li, G., & Zhu, X. (2019). Numerical study of solid particle erosion in a centrifugal pump for liquid–solid flow. *Journal of Fluids Engineering*, *141*(12) http://doi.org/10.1115/1.4043580

Li, J., Su, N., Wei, L., Zhang, X., Yin, Y., & Zhao, W. (2019). Study on the surface forming mechanism of the solid–liquid two-phase grinding fluid polishing pipe based on large eddy simulation. *Proceedings of the Institution of Mechanical Engineers. Part B, Journal of Engineering Manufacture*, *233*(14), 2505-2514. http://doi.org/10.1177/0954405419841814

Li, R., Sun, Z., Li, A., Li, Y., & Wang, Z. (2022a). Design optimization of hemispherical protrusion for

mitigating elbow erosion via CFD-DPM. *Powder Technology*, *398*, 117128. http://doi.org/10.1016/j.powtec.2022.117128

Li, Y., Du, J., Lan, Y., Du, H., & Huang, H. (2022b). Numerical analysis of the factors influencing the erosion of the valve port of a high-speed on/off valve. *Applied Sciences*, *12*, 6212. http://doi.org/10.3390/app12126212

Lin, Z., Sun, X., Yu, T., Zhang, Y., Li, Y., & Zhu, Z. (2020). Gas–solid two-phase flow and erosion calculation of gate valve based on the CFD-DEM model. *Powder Technology*, *366*. http://doi.org/10.1016/j.powtec.2020.02.050

Liu, E., Li, D., Li, W., Liao, Y., Qiao, W., Liu, W., & Azimi, M. (2021). Erosion simulation and improvement scheme of separator blowdown system ——A case study of Changning national shale gas demonstration area. *Journal of Natural Gas Science and Engineering*, *88*, 103856. http://doi.org/10.1016/j.jngse.2021.103856

Morsi, S., & Alexander, A. (1972). An investigation of particle trajectories in two-phase flow systems. *Journal of Fluid Mechanics*, *55*(2), 193-208. https://doi.org/10.1017/S0022112072001806

Ou, G., Luo, M., Gu, Y., & Jin, H. (2022). Study on erosion-wear characteristics of bidirectional metal seal floating ball valve in liquid-solid two-phase flow environment. *Proceedings of the Institution of Mechanical Engineers, Part C: Journal of Mechanical Engineering Science*, 2141040459. http://doi.org/10.1177/09544062221125333

Ou, G., Ouyang, P., Zheng, Z., Jin, H., Bie, K., & Wang, C. (2018). Investigation on failure process and structural improvement of a high-pressure coal water slurry valve. *Engineering Failure Analysis*, *96*. http://doi.org/10.1016/j.engfailanal.2018.09.003

Ri, J., Ripeanu, R., & Dinita, A. (2020). Erosion modeling in parallel gate valve. *Fme Transactions*, *48*(4), 808-815. http://doi.org/10.5937/fme2004808H

Singh, H., Kumar, S., & Mohapatra, S. (2020). Modelling of solid-liquid flow inside conical diverging sections using computational fluid dynamics approach. *International Journal of Mechanical Sciences*, *186*. http://doi.org/10.1016/j.ijmecsci.2020.105909

Tang, C., & Kim, Y. (2020). CFD-DEM simulation for the distribution and motion feature of solid particles in single-channel pump. *Energies*, *13*(19), 4988. http://doi.org/10.3390/en13194988

Tokura, Y., Uddin, M. A., & Kato, Y. (2019). Effect of suspension pattern of sedimentary particles on solid/liquid mass transfer in a mechanically stirred vessel. *Industrial & Engineering Chemistry Research*, *58*(24), 10172-10178. http://doi.org/10.1021/acs.iecr.9b00594

Xu, B., Lin, Z., Zhu, Z., & Yu, T. (2022). Experimental and simulation study of the effect of gravity on the solid-liquid two-phase flow and erosion of ball valve. *Advanced Powder Technology*, *33*, 103416. http://doi.org/10.1016/j.apt.2021.103416

Yamamoto, Y., Potthoff, M., Tanaka, T., Kajishima, T., & Tsuji, Y. (2001). Large-eddy simulation of turbulent gas–particle flow in a vertical channel: Effect of considering inter-particle collisions. *Journal of Fluid Mechanics*, *442*, 303-334. https://doi.org/10.1017/S0022112001005092

Yang, T., Hong, Y., Wang, A., Ran, X., Fan, X., & Hu, C. (2021). Failure mechanism and optimization of throttle valve based on computational fluid dynamics. *International Journal of Heat and Technology*, *39*, 906-912. http://doi.org/10.18280/ijht.390325

Zhang, G., Xin, J., Chen, D., & Lin, Z. (2023). Numerical simulation of liquid–solid two-phase flow and erosion of Y-type slurry valve with different openings. *Proceedings of the Institution of Mechanical Engineers, Part E: Journal of Process Mechanical Engineering*. https://doi.org/10.1177/09544089231193233

Zhang, X., Chen, Y., & Yang, W. (2019). Erosion of an arrow-type check valve duo to liquid–solid flow based on computational fluid dynamics. *Journal of Failure Analysis and Prevention*, *19*(2), 570-580. http://doi.org/10.1007/s11668-019-00632-y

Zhang, Y., Liu, X., Li, B., Sun, S., Peng, J., Liu, W., He, J., & Wei, L. (2022). Hydrodynamic characteristics and optimization design of a bio-inspired anti-erosion structure for a regulating valve core. *Flow Measurement and Instrumentation*, *85*, 102173. http://doi.org/10.1016/j.flowmeasinst.2022.102173

Zhang, Y., Reuterfors, E. P., McLaury, B., Shirazi, S., & Rybicki, E. (2007). Comparison of computed and measured particle velocities and erosion in water and air flows. *Wear*, *263*, 330-338. http://doi.org/10.1016/j.wear.2006.12.048

Zheng, C., Liu, Y., Wang, H., Zhu, H., Liu, Z., Cai, B., & Shen, Y. (2015). Numerical study on improving the erosion life of ball seat for oil & gas reservoir fracturing. *Engineering Failure Analysis*, *60* http://doi.org/10.1016/j.engfailanal.2015.11.050